GEND
017

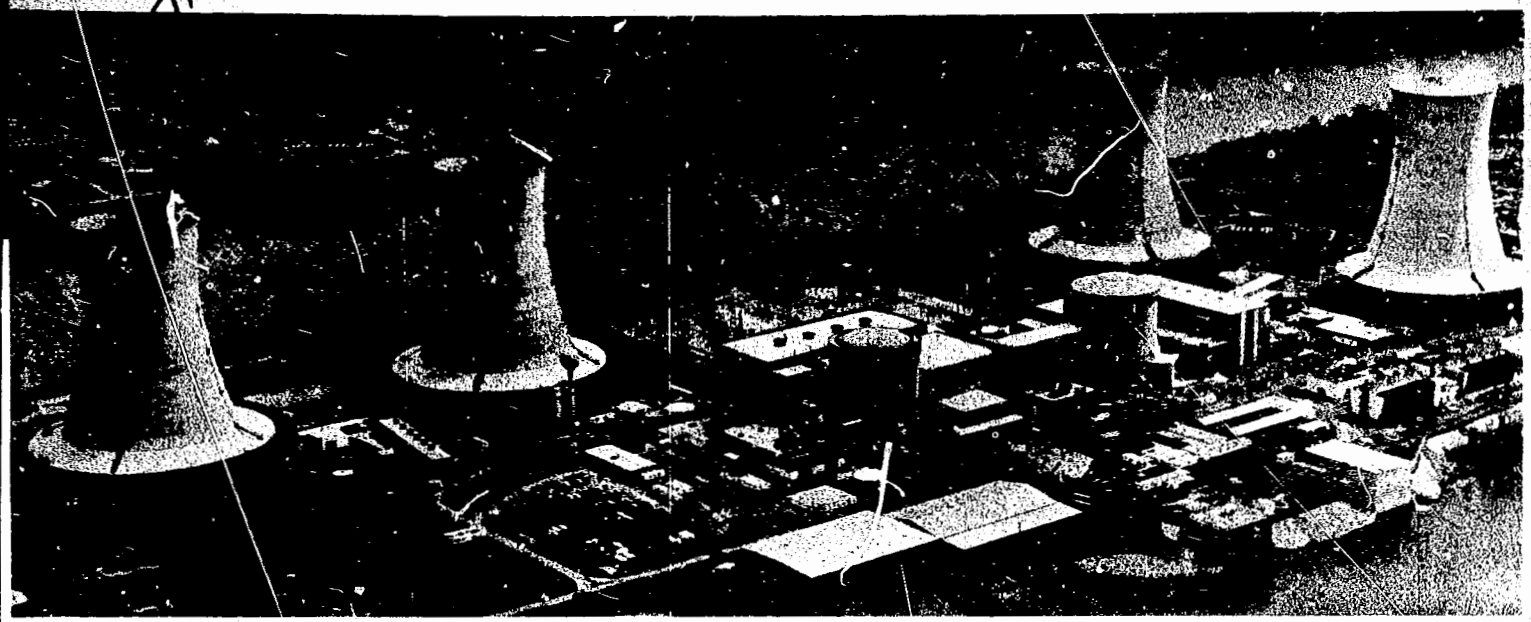

GEND

General Public Utilities • Electric Power Research Institute • U.S. Nuclear Regulatory Commission • U.S. Department of Energy

MASTER

# Response of the SPND Measurement System To Temperature During the Three Mile Island Unit 2 Accident


Ned Wilde
John L. Morrison, Jr.


December 1981


Prepared for the
U.S. Department of Energy
Three Mile Island Operations Office
Under DOE Contract No. DE-AC07-76IDO1570

GEND-017
Distribution Category: UC-78
TMI Supplement

# RESPONSE OF THE SPND MEASUREMENT SYSTEM TO TEMPERATURE DURING THE THREE MILE ISLAND UNIT 2 ACCIDENT

Ned Wilde
John L. Morrison, Jr.

Published December 1981

Technically Edited and Published
on Behalf of the GEND Group
by
EG&G Idaho, Inc.
Idaho Falls, Idaho 83415



Prepared for the
U.S. Department of Energy
Three Mile Island Operations Office
Under DOE Contract No. DE-AC07-76IDO1570

## ABSTRACT

The Self-Powered Neutron Detector (SPND) Measuring System is evaluated to determine its ability to indicate temperatures of the fuel rods in the TMI-2 reactor core during the accident. (The ability of the system to perform as specified is not a consideration.)

We conclude for the following reasons that the SPND Measuring System did not provide fuel rod temperatures during the accident.

1. The heat transfer characteristics vary over a range of five octaves.

2. Within the range of 1200 to 1800°F, the SPND responds to temperature from convection radiation from the fuel rods and self-heating from the gamma flux.

3. Within the range of 1200 to 1800°F, the signal cable introduces masking signals that are a function of gamma heating, integrated temperature over the cable, and core water level velocity.

4. The data system's worst-case signal-to-noise ratio from aliasing is 0dB.

5. The recorder system's worst-case signal-to-noise ratio from aliasing is -24dB.

ACKNOWLEDGMENTS

We wish to acknowledge the contribution of J. W. Mock, EG&G Idaho, Inc., for his overall guidance in the structure of this paper; A. K. Tyron-Hopko, EG&G Idaho, Inc., for her patience and able assistance with the presentation; D. R. Chick, EG&G Idaho, Inc., for his assistance with some of the technical details; R. O. Albertson, EG&G Idaho, Inc., for his able assistance with the test instrumentation.

CONTENTS

FIGURES

TABLES

## EXECUTIVE SUMMARY

This report technically examines in depth the possibility of extracting time-temperature profiles for the damaged TMI-2 reactor core during the accident, from data produced by the flux monitoring system. The flux monitoring system comprises self-powered neutron detectors (SPNDs) that are distributed throughout the reactor core in a three-dimensional array. It has been shown that in the temperature range of interest, 1200 to 1800°F, the SPNDs have a predictable temperature response that will provide signal levels compatible with the measurement system. Data from the TMI-2 flux monitoring system recorded during the accident indicate the presence of large signal levels about 2.5 hr after the initial scram. These large signal levels are not from neutron flux, and therefore must be from temperature. It is from this data that information on time-temperature profiles is desired.

The report shows that the desired time-temperature profiles in the core during the accident cannot be obtained from the flux monitor system data, for the following reasons:

1. The heat transfer characteristics from fuel rod to SPND are highly uncertain. This causes great difficulty in trying to relate fuel rod temperature to SPND temperature.

2. The signal from the SPND is summed with signals generated in the sheathed cable that provides electrical connections to the SPNDs. The cable signal is of the same magnitude as the SPND signal and a function of different variables, such as the average temperature along the length of the cable and the velocity at which the water level is falling along the cable. This spurious signal cannot be separated from the SPND temperature signal.

3. The dynamics of the SPND signal widely vary, due to a large variation in bandwidth of the sheathed cable caused by high temperatures.

4. Sample rates in the data system and multi-point recorder are such that signal-to-noise ratio of the data cannot be guaranteed to be any better than 0 db. In other words, the level of noise from aliasing is equal to the level of signal.

The report develops these conclusions thoroughly, covering such topics as heat transfer, SPND temperature response, cable effects, and an analysis of the sample data system.

# RESPONSE OF THE SPND MEASUREMENT SYSTEM TO TEMPERATURE DURING THE THREE MILE ISLAND UNIT 2 ACCIDENT

## INTRODUCTION

This report documents the results of a study undertaken at the request of the Technical Integration Office (TIO) at the Three Mile Island (TMI) Facility. The TIO is operated by EG&G Idaho for the Department of Energy. Its basic charge is to learn as much as possible from the aftermath of the TMI-2 accident as to how the various systems, subsystems, and components tolerated the accident. The various studies and tests are being performed in conjunction with the decontamination retrofit and requalification work being done on the facility. The information gathered by the TIO is public domain and will be disseminated to interested groups, such as utility operators, A&E firms, universities, and other groups expressing interest.

The specific question that initiated this study concerns the behavior of the flux monitoring system during the accident. The purpose of the flux monitoring system at TMI is to establish the shape of the neutron flux in the reactor core when it is at steady state power. The shape is established from data obtained by a three-dimensional array of point measurements of neutron flux distributed throughout the reactor core. These point measurements are made by self-powered neutron detectors (SPNDs).[a] The SPND is a rather small device used inside of reactor cores to measure local flux densities. It is an unpowered instrument that generates an electric current through the interaction of thermal neutrons with the sensitive portion of the SPND called the emitter. A sheathed cable, with aluminum oxide dielective, carries the signal current through the pressure boundary to a hard-to-soft splice and on to a data recovery system. The data system processes the SPND information and outputs information on the flux shape. When the reactor is shut down there is no neutron flux present and the SPNDs indicate no output. However, during the accident this was not the case. About 2.5 hr after the initial scram, the flux monitor system indicated very high signal

a. See Appendix A for vendor data on SPNDs.

levels. Figure 1 indicates a sketch of the data taken from the backup recorder. It has been shown[a] that above 700°F the SPND will start to generate a current that is a function of temperature. Since the reactor was shut down, these large levels of signals must have been from temperature effects.

Thus, the specific question asked by the TIO was whether the data from the flux monitor system could be utilized to obtain a three-dimensional time-temperature profile of the fuel rods in the reactor core that would provide information on the evolution of core damage. In order to address this specific question, a block diagram was conceived to analyze the flux monitoring system's behavior as a temperature monitoring system (see Figure 2). It illustrates how the flux monitoring system would have to transform fuel temperature information into information out of the data system and backup recorder. In order to ascertain fuel rod temperature from the SPND measurement system, the transfer characteristics for each block in the system must be precisely identified so the fuel temperature information can be determined from the recorded output. This report follows the structure of the block diagram of Figure 2. In general, each block will be analyzed in detail by a section of this report. The attempt is to try to bound each block's transfer characteristics and establish its uncertainties. The first three blocks are analyzed over the temperature range of 650 to 1800°F. The response of Blocks 4, 5, and 6 is based on the SPND being at moderate temperatures (1000°F), which was not always the case. This approach is argued to be valid because it will be shown that at moderate temperatures the transfer characteristics of Blocks 4, 5, and 6 establish unacceptably high uncertainties, whereas at high temperatures, the transfer characteristics of Blocks 1, 2, and 3 establish unacceptably high uncertainties. Thus, it will be shown impossible to obtain temperature-time profiles from the SPND accident data with any acceptable levels of uncertainty.

---

a. Work by Babcock & Wilcox; see Appendix B.

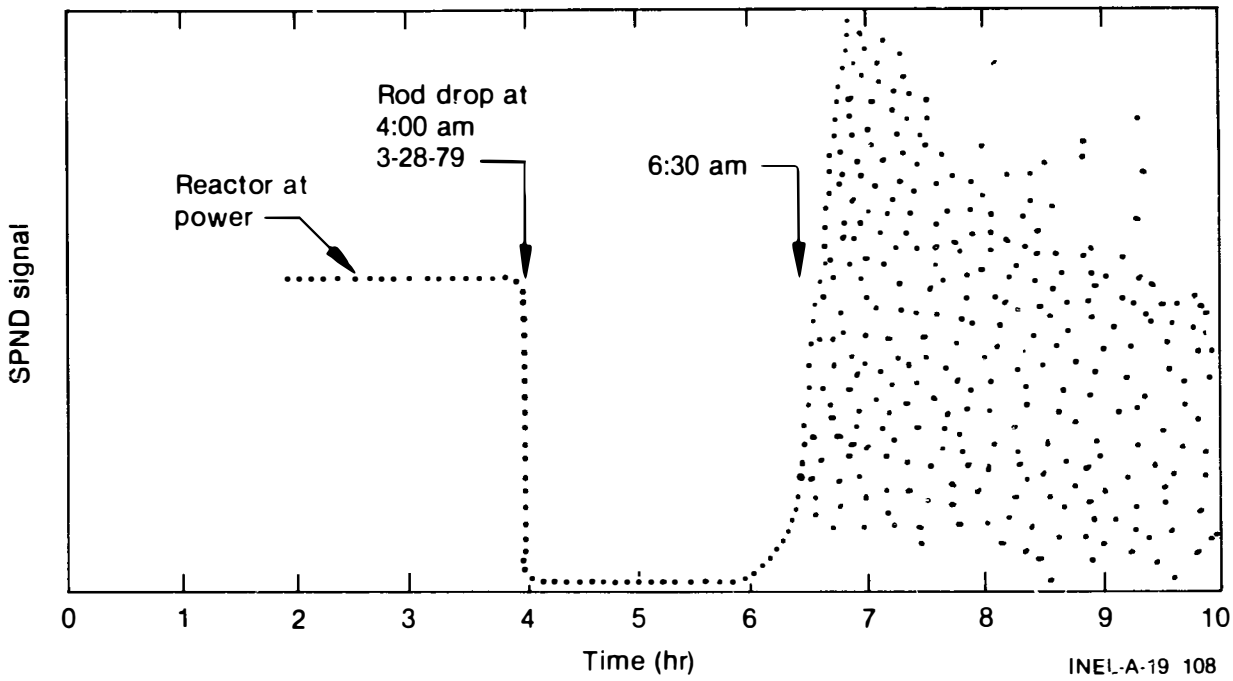


Figure 1. Backup recorder's tracing of in-core detector signals.

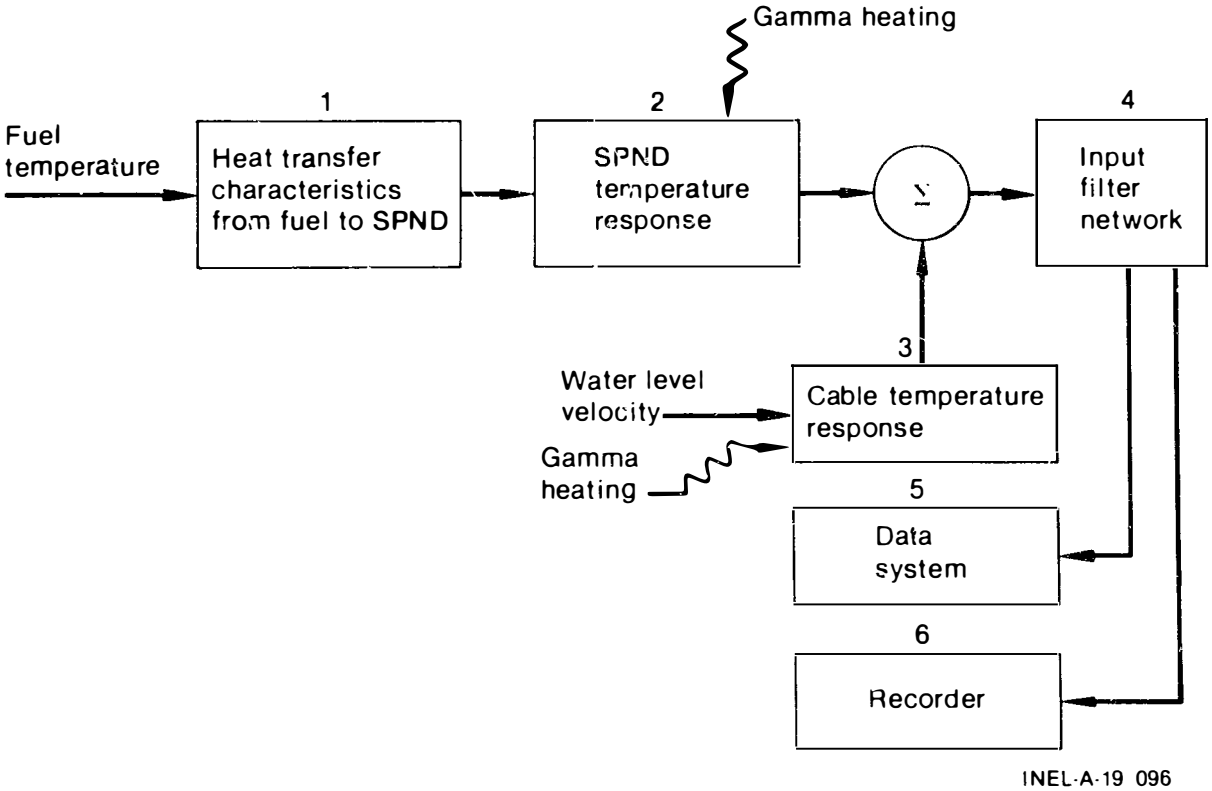


Figure 2. Block diagram of SPND measurement system for measuring fuel rod temperature.

## HEAT TRANSFER CHARACTERISTICS FROM FUEL TO THE SPND

### Core Environment

The normal operating condition of the TMI-2 reactor is approximately 582°F (average) at a pressure of 2155 psig. After the accident, the reduced pressure allowed boiling. Over time, the level of the boiling water dropped below the top of the core. Thus, at the beginning, the heat transfer from fuel to SPND was through boiling water. As the level dropped further, a given elevation would be a transition region consisting of the surface of the boiling water, steam, and gas. The gas would probably be a mixture of hydrogen and fission gases. The water must have been churning such that alternate heating and quenching of the fuel and detector surface was taking place. Later, this elevation would be in a steam or gas-steam mixture. The purpose of this section is to scope and bound the heat transfer characteristics during this time. This is not an attempt to model or define these characteristics.

### Core Geometry

The 12-ft core has 177 fuel assemblies. Each assembly has 225 positions in a 15 by 15 lattice consisting of 208 fuel rods, 16 control rods, and one instrument tube in the center. Each fuel rod is 0.430 in. in diameter and each instrument tube is 0.493 in. in diameter, with 0.088 in. spacing between rods and tubes. Fifty-two of the instrument tubes contain seven SPND flux detectors distributed uniformly over the 12-ft vertical height of the core. These 364 SPND yield axial flux shape and level information. Each instrument tube has fuel rods in the eight adjacent positions. Both the fuel rods and instrument tubes have zircaloy-4 surfaces. Figure 3 summarizes this information.

### Heat Transfer: Convection/Conduction Path

Figure 4 illustrates the various heat transfer modes. The fuel rod is the heat source having temperature $T_R$, and the instrument tube is the heat sink having temperature $T_D$, which means $T_R > T_D$. The SPND is

Core Geometry

Fuel assemblies in core: 177

Positions in fuel assemblies: 15 x 15 = 225

52 assemblies contain
- 208 Fuel rods
- 16 Control rods
- 1 SPND instrument tube

225

Total SPND: 52 x 7 = 364

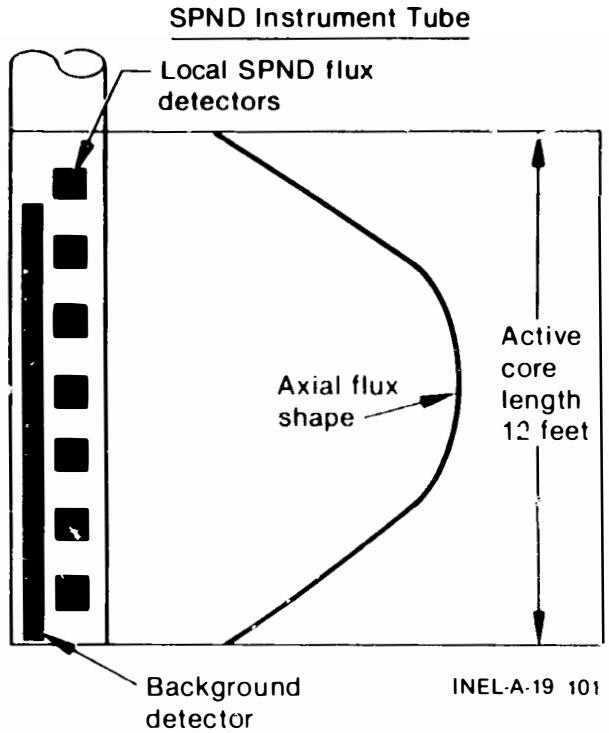


Figure 3. In-core neutron flux monitoring system.

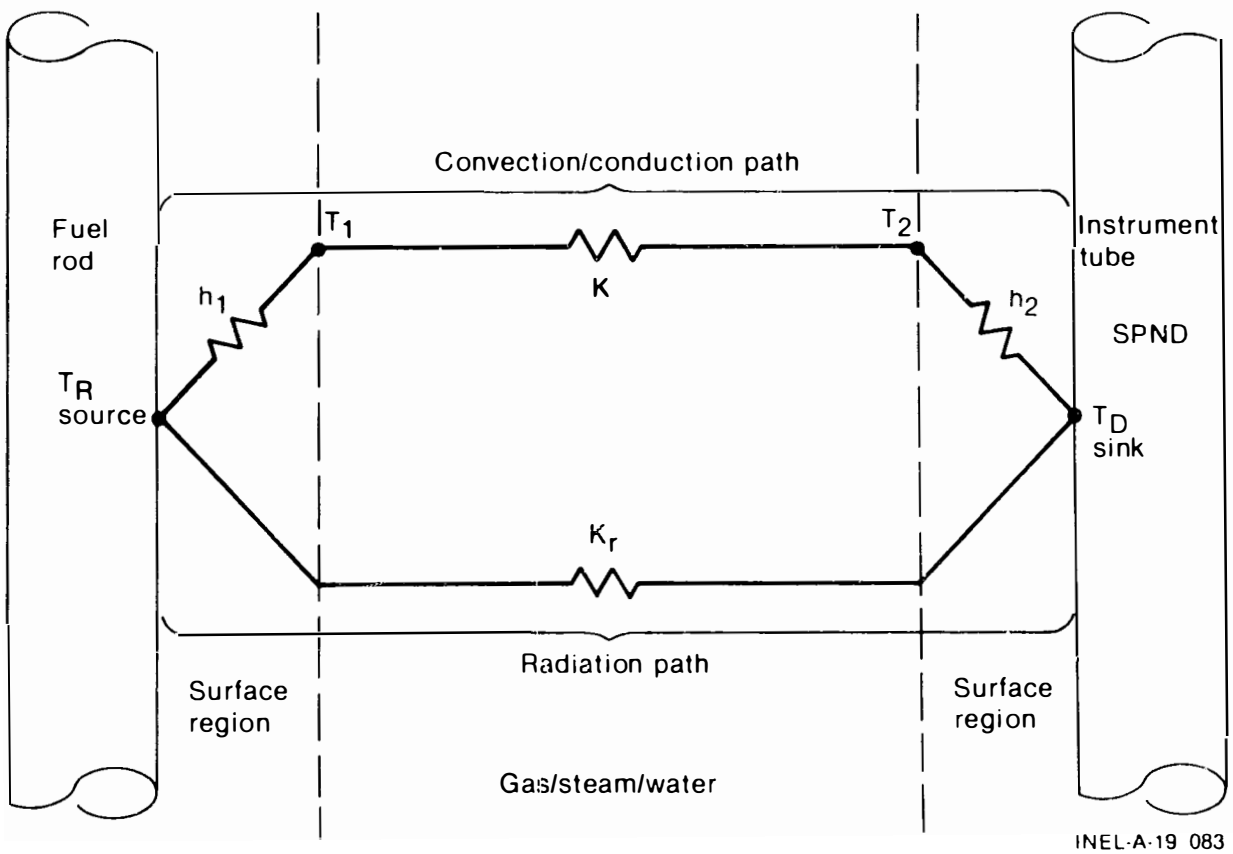


Figure 4. Heat transfer modes.

assumed to be at temperature $T_D$. The figure assumes a plain, one-dimensional steady-state linear model where $\bar{q}$ is the heat flux.

The convection/conduction path $K_c$ is composed of three elements. The heat transfer through the surface regions (which is considered very thin) is described by the heat transfer coefficient (or surface conductivity) h as follows:

$$\bar{q}_{h_1} = h_1(T_R - T_1)$$

and

$$\bar{q}_{h_2} = h_2(T_2 - T_D) \quad . \tag{1}$$

The convection/conduction transfer through the medium is described using the thermal conductivity K as follows:

$$\bar{q}_K = \frac{K}{X}(T_1 - T_2) \tag{2}$$

where X is the distance between rod and tube.

The heat flux flowing from the source to the sink through the convection/conduction path must be the same through each of these elements:

$$\bar{q}_c = \bar{q}_{h_1} = \bar{q}_K = \bar{q}_{h_2} \tag{3}$$

which is equal to

$$\bar{q}_c = \frac{T_R - T_D}{\frac{1}{K/X} + \frac{1}{h_1} + \frac{1}{h_2}} \quad . \tag{4}$$

There is no reason to expect conditions at the rod surface to be different from conditions at the tube surface. The material is the same and the spacing small. Therefore, assume that

$$h = h_1 = h_2 \ . \tag{5}$$

Also, let

$$\Delta T = T_R - T_D \tag{6}$$

and remember that X = 0.00733 ft. Then

$$\bar{q}_c = K_c \Delta T \tag{7}$$

where

$$K_c = \left( \frac{1}{136\ K} + \frac{2}{h}^{-1} \right).$$

This describes the heat flux transferred through the convection/conduction path.

A valid question can be raised concerning the conduction element in this path. The inclusion of the conduction element in series with the two convection elements may not be justifiable due to the presumed well-mixed nature of the heat transfer medium. In other words, if temperature $T_1$ equals temperature $T_2$, then the thermal resistance is zero, or the conductivity K is infinite. However, its inclusion has the effect of reducing the uncertainties in this path and hence will be used. This results in a more conservative analysis.

## Heat Transfer: Radiation Path

The heat flux transferred through the radiation path is a little simpler to describe:

$$\bar{q}_r = K_r \, \Delta T \tag{8}$$

where

$$K_r = \frac{\sigma F (T_R^4 - T_D^4)}{(T_R - T_D)}$$

and

$\sigma$ = the Stefan-Boltzmann constant $1.714 \times 10^{-9} (Btu/hr/ft^2/°R^4)$

F = a module which modifies $K_r$ to account for the emittances, relative geometry factor of the rod(s), and tube and attenuation in the heat transfer medium.

Now the total heat flux per degree Fahrenheit is

$$\phi = K_c + K_r (Btu/hr/ft^2/°F) \tag{9}$$

Note: Degrees Roentgen (°R) = 459.7 + degrees Fahrenheit (°F), and represents absolute zero on the Fahrenheit scale.

## Numerical Values

The next step is to bound the numerical values of the coefficients used. Table 1 gives various values for the thermal conductivity (K) of gas, steam, and water at various temperatures of interest.[1] Values for the heat transfer coeffiecient (h) are more difficult to define since it is a very complicated process, a function of many parameters. Only a broad range of values can be given for the general case as indicated in Table 2. These values are only ballpark figures, but are the best that can be done without more specific information. Remember, the intent is to bound the heat transfer characteristics.

TABLE 1. RANGE OF THERMAL CONDUCTIVITIES (K)

| Temperature (°F) | K(Btu/hr/ft$^2$/°F) | | |
|---|---|---|---|
| | Gas | Steam | Water |
| 212 | 0.018 | 0.015 | 0.40 |
| 650 | 0.025 | 0.025 | 0.30 |
| 1200 | 0.035 | 0.045 | -- |
| 1800 | 0.045 | 0.065 | -- |

TABLE 2. ORDER OF MAGNITUDE OF HEAT TRANSFER COEFFICIENTS (h)

| Coolant | Range h(Btu/hr/ft$^2$/°F) |
|---|---|
| Gas, free convection | 1 to 5 |
| Superheated steam or gas, forced convection | 5 to 50 |
| Water, forced convection | 50 to 2 000 |
| Water, boiling | 500 to 10 000 |
| Steam, condensing | 1 000 to 20 000 |

The heat transfer coefficient ($K_c$) for the convection/conduction path can be calculated for the various conditions. Table 3 presents these calculations.

Table 4 gives the corresponding values for the radiation path heat transfer coefficients for various temperature differences for the case of F = 1. It will be assumed that the fuel rod surface and the detector tube are near the same temperature but still $T_R > T_D$. This means that the table values on the diagonal are of greatest interest. These values must be modified for various other effects. First, the geometry shape factor describes the amount of radiant heat flux seen by the heat sink. Since the instrument tube is surrounded by fuel rods, this factor should be high. A value of 0.8 is selected. The second factor is the emittance of the surface, which is a function of temperature, wavelength, roughness, scaling, and others. This factor can vary over a wide range. Values from 0.4 to 0.8 have been selected as typical. The third effect is the absorption, reflection, and reradiation by gas, steam, and water. Here again, this is a

TABLE 3. OVERALL HEAT TRANSFER COEFFICIENTS (K) FOR THE CONVECTION/CONDUCTION PATH

$$K_c = \left(\frac{1}{136K} + \frac{2}{h}\right)^{-1} \text{(Btu/hr/ft}^2\text{/°F)}$$

| Coolant | Temperature °F | Temperature K(Btu/hr/ft$^2$/°F) | Value of $K_c$ (Btu/hr/ft$^2$/°F) h = 1 | Value of $K_c$ (Btu/hr/ft$^2$/°F) h = 2 |
|---|---|---|---|---|
| Gas, free convection | 212 | 0.018 | 0.42 | 1.2 |
| | 600 | 0.025 | 0.44 | 1.4 |
| | 1200 | 0.035 | 0.45 | 1.6 |
| | 1800 | 0.045 | 0.46 | 1.8 |
| Gas, forced convection | 212 | 0.018 | 1.2 | 2.2 |
| | 600 | 0.025 | 1.4 | 3.0 |
| | 1200 | 0.035 | 1.6 | 4.0 |
| | 1800 | 0.045 | 1.8 | 4.9 |
| Steam, superheated forced convection | 212 | 0.015 | 1.1 | 1.9 |
| | 600 | 0.025 | 1.4 | 3.0 |
| | 1200 | 0.045 | 1.8 | 4.9 |
| | 1800 | 0.065 | 2.0 | 6.5 |
| Steam, condensing | 212 | 0.015 | 2.0 | 2.0 |
| | 600 | 0.025 | 3.4 | 3.4 |
| | 1200 | 0.045 | 6.1 | 6.1 |
| | 1800 | 0.065 | 8.7 | 8.9 |
| Water, forced convection | 212 | 0.40 | 50 | 2 000 |
| | 600 | 0.30 | 17 | 52 |
| | 1200 | -- | 16 | 39 |
| | 1800 | -- | -- | -- |
| Water, boiling | 212 | 0.40 | 500 | 10 000 |
| | 600 | 0.30 | 54 | 54 |
| | 1200 | -- | 35 | 41 |
| | 1800 | -- | -- | -- |

function of temperature, wavelength, geometry, and density of the medium. Little radiation will be transmitted through the water. Select a value range of 0.01 to 0.1. For steam, select a value range of 0.1 to 0.9, and for air, which will pass essentially all radiant heat use, a value of 1.0. Multiplying these three factors together will give a crude estimate of the range of F.

TABLE 4. HEAT TRANSFER COEFFICIENTS FOR THE RADIATION PATH (TABLE VALUES FOR THE CASE OF F = 1)

$$K_r = 1.714 \times 10^{-9} F \frac{(T_R^4 - T_D^4)°R}{(T_R - T_D)°F} \text{ (Btu/hr/ft}^2\text{/°F)}$$

| | $T_R$ | | | |
|---|---|---|---|---|
| TD (°F) | 212 (°F) | 600 (°F) | 1200 (°F) | 1800 (°F) |
| 212 | 2.1 | 5.1 | 13 | 28 |
| 600 | -- | 9.4 | 19 | 37 |
| 1200 | -- | -- | 31 | 53 |
| 1800 | -- | -- | -- | 79 |

All the information from Tables 3, 4, and 5 have been consolidated in the bar graph of Figure 5. The length of the bar shows the uncertainty associated with each type of heat transfer mechanism. Below the water level, the temperature will be below 600°F, and the heat transfer will be through the conductive path. Above the water level, where a steam or a gas-steam mixture is expected, and the temperature range of interest is 1200 to 1800°F, the heat transfer will be through the radiation path. In the vicinity of the water surface, where gas, steam, and water may be mixed, the major path would be uncertain indeed.

TABLE 5. RANGE OF VALUES FOR F

| | |
|---|---|
| Gas | 0.3 to 0.6 |
| Steam | 0.03 to 0.6 |
| Water | 0.003 to 0.06 |

## Conclusion

It has been suggested that the SPND might be used as a temperature sensor that would provide information on the time history of the fuel temperature. But even if the SPND were the ideal temperature sensor and the

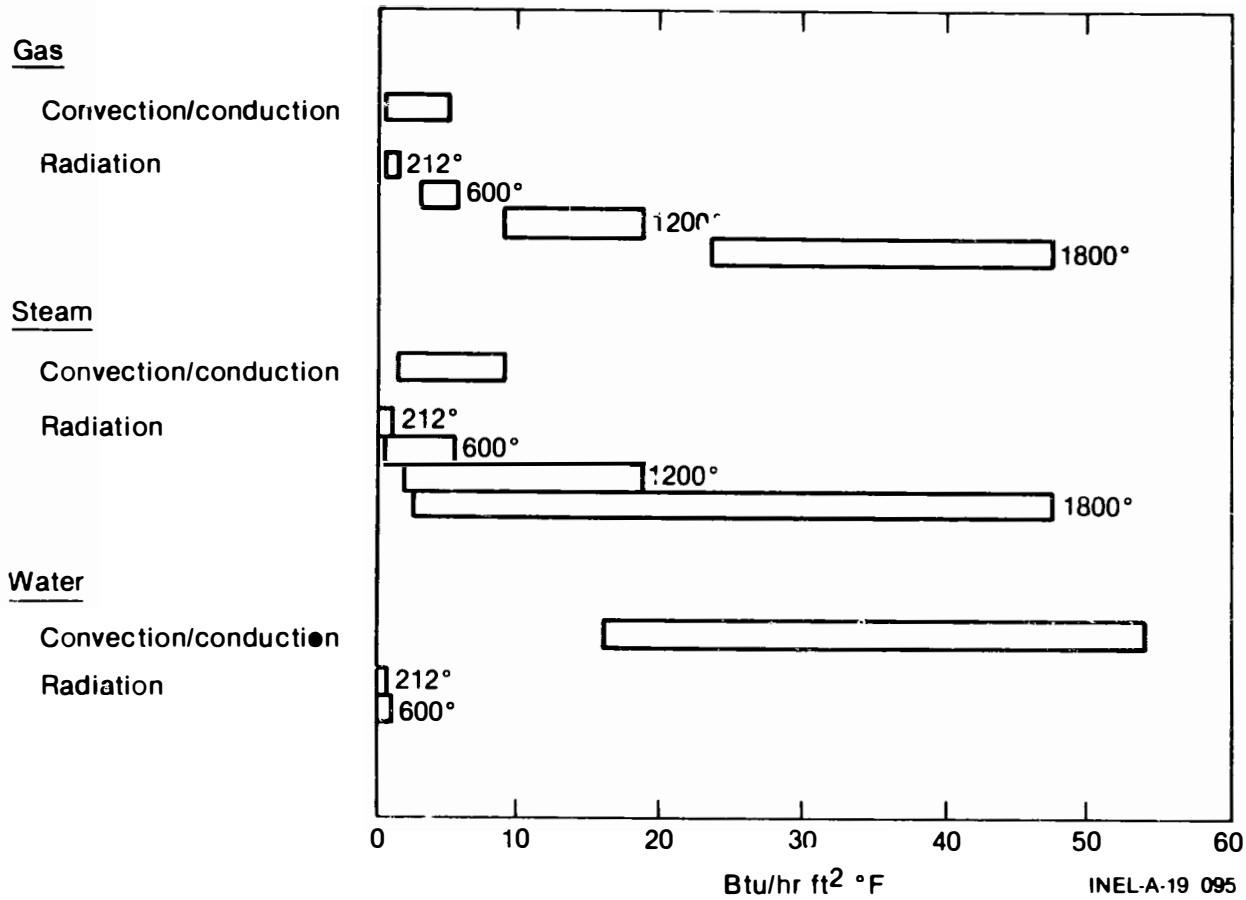


Figure 5. Uncertainty range of heat transfer coefficients.

temperature history were completely known at the SPND, the fuel temperature history would be lost. The region of interest would be above the water in the steam or gas-steam mixture and in the 1200 to 1800°F range, where the radiation heat transfer path dominates. Unfortunately, this transfer mechanism has the greatest uncertainty due to the many unknown parameter values. The lack of knowledge of the heat transfer properties completely masks the fuel temperature history.

## GAMMA HEATING OF THE SPND

The heat output of the TMI-2 reactor core is approximately 3000 MW (thermal). After a sustained period of operation, the gamma energy release rate will be approximately 0.5% of this power 2.5 hr after shutdown and 0.06% after 30 days. An SPND instrument tube occupies about $2.5 \times 10^{-3}$% of the core volume. Making the conservative assumption that gamma absorption is the same in both a fuel rod and an instrument tube, the tube would dissipate 380 W at 2.5 hr and 45 W at 30 days. Both the SPND and the cable would experience this heating.

The resulting temperature rise in the tube cannot be determined since the rate of heat transfer to the cooling medium is poorly known (see Heat Transfer Characteristics From Fuel to the SPND, above). However, any additional heat source such as this gamma heating only tends to mask the temperature information being sought.

## SPND TEMPERATURE CHARACTERISTICS ANALYSIS

### SPND Environment

In the TMI-2 reactor, the distribution of the core neutron flux is continuously measured by the incore monitoring system. The measurements are provided by 52 detector assemblies located throughout the core. Each detector assembly contains seven SPNDs plus various other detectors. The seven SPNDs are positioned vertically at seven core axial elevations over the 12-ft active core length. Data from each of these 364 SPNDs is transmitted out of the core by electrical cables and then to the plant computer system. Within the core, the cables are vertical.

The SPND is designed to be a neutron detector; however, it also has an electrical output that is a function of temperature. At the normal operating temperature of approximately 600°F, this temperature-induced output is presumed negligible compared to the neutron-induced output. Now in the TMI-2 accident, the neutron activity was not a major factor in the environment of the SPND after the initial few minutes. As the water level lowered, the SPND environment could reach the 1200 to 1800°F region. The resulting output can then be considered a function of temperature only. This section investigates the SPND detector and cable system as a temperature detector.

### SPND Equivalent Circuit

There are four major temperature characteristics of concern in the 1200 to 1800°F range. These are

1. $I_T$, SPND thermionic current

2. $R_L$, SPND shunt insulations resistance

3. $I_D$, Cable temperature response (dielectric thermal relaxation charge)

4. $C_D$, Cable shunt capacitance.

The equivalent circuit diagram is shown in Figure 6:

These four characteristics are described in detail in a Babcock & Wilcox paper, included as Appendix B. Following is a summary of these items.

## Thermionic Current

In the 1200 to 1800°F region, a temperature-induced current is present, represented by an equivalent current source having the relationship

$$I_T = -10^{-8} e^{+0.01334(T - 1200)} \tag{10}$$

where

$I_T$ = thermionic current in amperes

$T$ = temperature in °F ($1200 < T < 1800$).

This empirical expression was obtained by curve-fitting laboratory experiment data.

## Shunt Resistance

Also present is a leakage resistance that varies with temperature. The expression for this variation in the 1200 to 1800°F range is

$$R_L = 3 \times 10^6 e^{-0.01367(T - 1200)} \tag{11}$$

where

$R_L$ = leakage resistance in Ω

$T$ = temperature in °F ($1200 < T < 1800$).

This relationship was also obtained from experimental data.

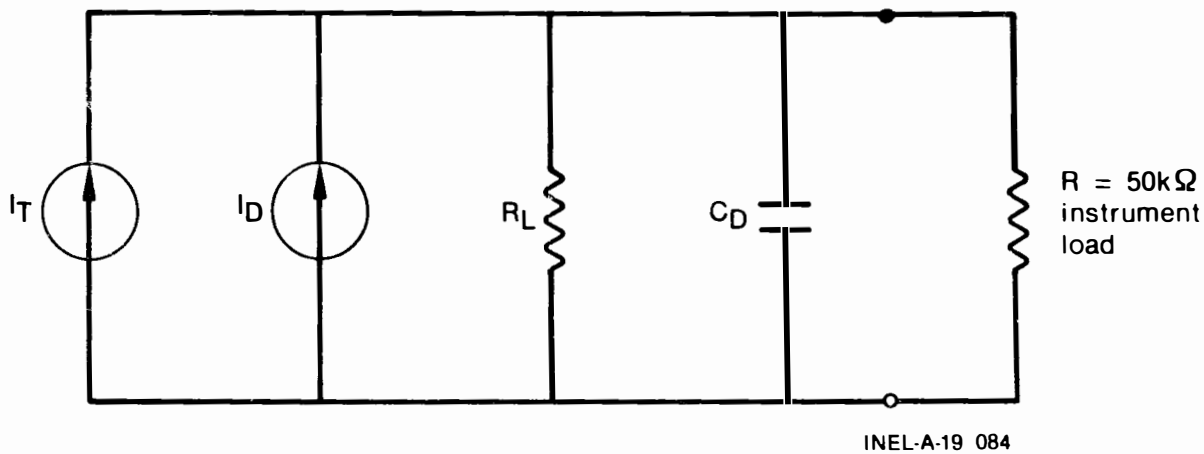


Figure 6. SPND equivalent circuit.

## SPND OUTPUT CURRENT

The SPND current source and temperature-dependent shunt resistance will give rise to a current in the 50K Ω instrumentation load resistance. This current is

$$(I_t)out = \frac{R_L}{R_L + R} I_t \quad . \tag{12}$$

This expression represents the temperature response of the SPND. The instrumentation full-scale current is 2000 nA. Table 6 presents values for the previous relationships.

TABLE 6. SPND OUTPUT CURRENT

| Temperature (°F) | $I_t$ (MA) | $R_L$ (KΩ) | R (KΩ) | $(I_t)$out (MA) |
|---|---|---|---|---|
| 1200 | -10 | 3000 | 50 | -9.84 |
| 1300 | -38 | 765 | 50 | -35.6 |
| 1400 | -144 | 195 | 50 | -115 |
| 1500 | -547 | 49.7 | 50 | -273 |
| 1600 | -2080 | 12.7 | 50 | -420 |
| 1700 | -7880 | 3.23 | 50 | -478 |
| 1800 | -29900 | 0.822 | 50 | -484 |

### Cable Temperature Response (Dielectric Thermal Relaxation Charge)

As the aluminum oxide dielectric is heated to these higher temperatures, electrons are released and produce a positive current. This is a one-time effect and a function of the temperature's integrated time history. Measured average value of the charge available ($Q_A$) for release is approximately 4 x $10^{-4}$ coulombs per foot (C/f) over the 12-ft detector. When the material is heated rapidly, the total charge is released in approximately one minute. A model for the release of the available charge per unit length as a function of time is

$$\frac{dQ}{dt} = Kt \quad e^{-at} \tag{13}$$

where

Q = released charge

K = constant determined by total charge available for release

a = reciprocal time constant.

For (1/a) = 10 s, this function appears as illustrated in Figure 7.

It has been assumed that, on the average, water boiled down in the core as a linear function of time. Thus, as a $\Delta X$ increment of detector length is exposed, it is heated rapidly and the charges released. Consider a $\Delta X$ increment located a distance $X_i$ from the top of the 12-ft detector and just above the water line. The released charge from this ith increment is

$$\left(\frac{dQ}{dt}\right)_i = K\ t_i\ e^{-a\ t_i}\ \Delta X \tag{14}$$

where $t_i$ is the time for the water to reach this level and the time that the ith charge release function starts. Since the velocity V is constant, $t_i$ can be replaced by Xi/V:

$$\left(\frac{dQ}{dt}\right)_i = K\ \frac{X_i}{V}\ e^{-aXi/V}\ \Delta X \quad . \tag{15}$$

By adding the contributions from all higher increments, a total current is obtained:

$$I = \sum \left(\frac{dQ}{dt}\right)_i \tag{16}$$

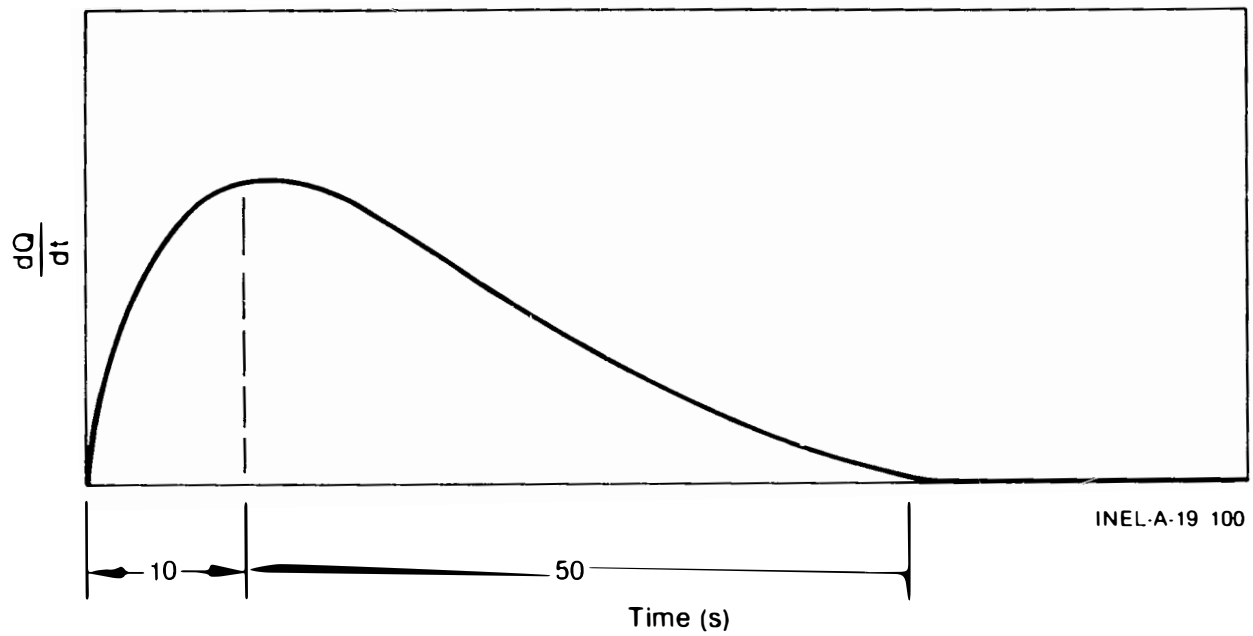


Figure 7. Charge Release Function.

$$I = \frac{K}{V} \sum_{i=0}^{L/\Delta X} x_i \, e^{-ax_i/V} \, \Delta X \quad . \tag{17}$$

Letting $\Delta X \to dx$, the limiting integral becomes

$$i(X) = \frac{K}{V} \int_0^L X \, e^{-aX/V} \, dX \quad . \tag{18}$$

Let $t_L = L/V$, the time required for the water to reach its present level ($X = L$). Now, changing variables,

$$I_D = K/V \int_0^{t_L} t \, e^{-at} \, dt \tag{19}$$

and integrating,

$$I_D = \frac{KV}{a^2} [1 - (at_L + 1) \, e^{-at_L}] \quad . \tag{20}$$

The constant K can be evaluated by equating the total released charge per unit length to the total available charge per unit length:

$$\int_0^\infty K \, t \, e^{-at} dt = Q_A \quad . \tag{21}$$

From which

$$K = a^2 \, Q_A . \tag{22}$$

The final expression is then

$$I_D = Q_A V[1-(at_L + 1) e^{-at_L}] \tag{23}$$

and describes the dielectric thermal relaxation charge current generator. For the suggested values of $Q_A = 4 \times 10^{-4}$ C/f and $(1/a) = 10$ s,

$$I_D = 4 \times 10^{-4} V \left[1 - \frac{t_L}{10} + 1\right] e^{-t_L/10} \quad . \tag{24}$$

For $t_L >> 10$ s (steady state),

$$I_D = QAV$$

or

$$I_D = 4 \times 10^{-4} (C/f) \frac{V(ft/hr)}{3600(s/hr)} \quad . \tag{25}$$

Note that this steady state current is a function only of the charge per foot available for release and the average velocity at which the water level is falling. Table 7 presents a range of values. This information may be easier to visualize if presented in terms of the length of the detector exposed above the water and the length of time it took to expose the detector assuming constant velocities. Table 8 is of this form.

TABLE 7. CABLE DIELECTRIC RELAXATION CURRENT AS A FUNCTION OF VELOCITY

| Velocity (ft/h) | Current (μA) |
|---|---|
| 0.1 | 0.011 |
| 0.3 | 0.033 |
| 1 | 0.11 |
| 3 | 0.33 |
| 10 | 1.1 |

TABLE 8. SPND DIELECTRIC RELAXATION CURRENT IN μA

| Time | Exposed Length (ft) 3 | 6 | 9 | 12 |
|---|---|---|---|---|
| 1 hr | 0.33 | 0.67 | 1.0 | 1.3 |
| 12 hr | 0.028 | 0.056 | 0.083 | 0.011 |
| 1 day | 0.014 | 0.028 | 0.042 | 0.056 |
| 2 day | 0.0065 | 0.014 | 0.021 | 0.028 |

## Cable Output Current

The cable current source and temperature-dependent shunt resistance will give rise to a second current in the 50 KΩ instrumentation load resistance. This current is

$$(I_D)_{out} = \frac{R_L}{R_L + R} I_D \quad . \tag{26}$$

Table 9 presents these values.

TABLE 9. CABLE OUTPUT CURRENT
($I_D$ CALCULATED FOR A VELOCITY OF 1 ft/hr)

| Temperature (°F) | $I_D$ (mA) | $R_L$ (K) | R (K) | $I_{Dout}$ (mA) |
|---|---|---|---|---|
| 1200 | 111 | 3000 | 50 | 109 |
| 1300 | 111 | 765 | 50 | 104 |
| 1400 | 111 | 195 | 50 | 88.4 |
| 1500 | 111 | 49.7 | 50 | 55.4 |
| 1600 | 111 | 12.7 | 50 | 22.5 |
| 1700 | 111 | 3.23 | 50 | 6.74 |
| 1800 | 111 | 0.822 | 50 | 1.80 |

## Total Output Current

The total current to the instrumentation system is

$$I_{out} = (I_T)_{out} + (Io)_{out} \quad . \tag{27}$$

Figure 8 is a plot of the component output currents. Both currents are within the 2000-mA full-scale value of the data system. It should be noted that the SPND output current is negative, though the cable output current is positive; hence, they tend to cancel each other.

## SPND-Cable Time Constant

The detector assembly shunt capacitance ($C_D$) increases from 96 pF/ft to 83 μF/ft as the temperature reaches the 1200 to 1800°F range. The length of this assembly is 12 ft. The length that is exposed to these high temperatures is that length that is above the water level; thus, as the water level lowered, the total shunt capacitance increased with time.

This large capacitance and the leakage resistance form a single-pole low-pass filter. Table 10 gives the time constant of this filter as a function of temperature and exposed length. Figure 9 is a graphic display of this data. The expression for the time constant is

TABLE 10. SPND-CABLE TIME CONSTANT

| Temperature (°F) | Exposed Length (ft) | | | |
|---|---|---|---|---|
| | 3 | 6 | 9 | 12 |
| 1200 | 12.25 | 24.49 | 36.74 | 48.98 |
| 1300 | 11.69 | 23.37 | 35.06 | 46.74 |
| 1400 | 9.908 | 19.82 | 29.72 | 39.63 |
| 1500 | 6.204 | 12.41 | 18.61 | 24.82 |
| 1600 | 2.515 | 5.031 | 7.546 | 10.06 |
| 1700 | 0.7547 | 1.509 | 2.264 | 3.019 |
| 1800 | 0.2014 | 0.4029 | 0.6043 | 0.8058 |

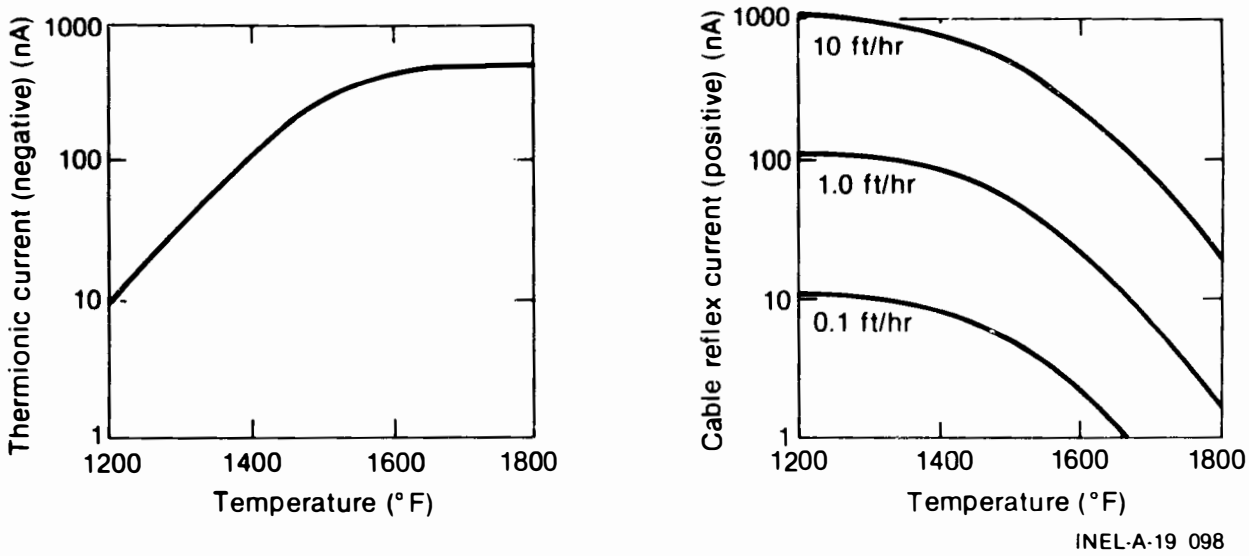


Figure 8. SPND and cable output current.

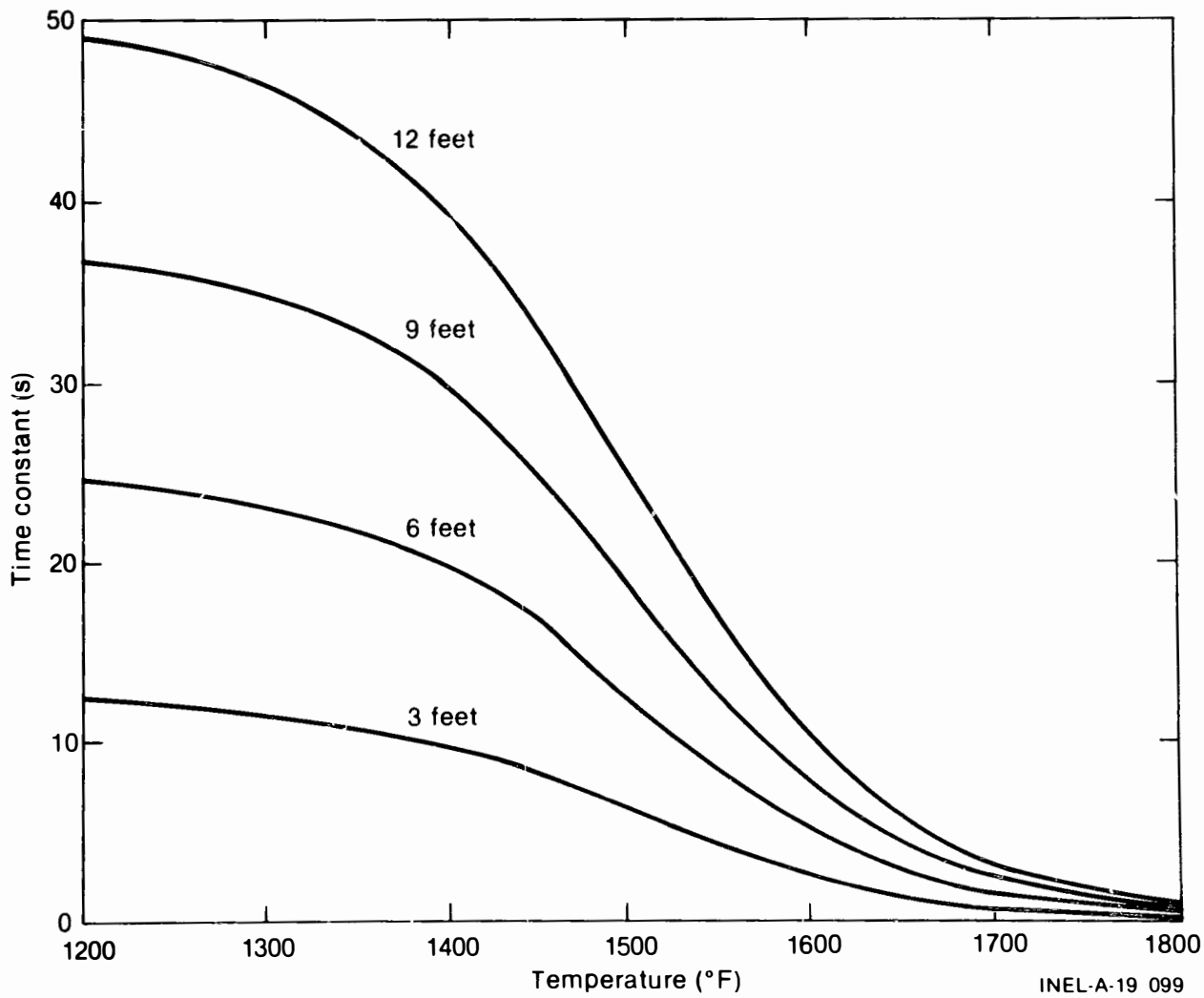


Figure 9. SPND-cable-time constant.

$$T = \frac{R_L \quad R}{R_L + R} C_D L \tag{28}$$

where

$C_D$ = 83 μF/ft

L = the exposed length in ft.

## Conclusion

We conclude the following:

1. The SPND thermionic current is reasonable and well-behaved when loaded with a 50K Ω resistance. The SPND temperature could be determined from the resulting current.

2. The cable thermal relaxation current is approximately the same order of magnitude and opposite sign as the thermionic current. This cable current is a function of time, vertical distance, and the integral of temperature.

3. The data system sees the sum of these two currents, and there is no practical way of separating them.

4. The long time constant due to the large cable capacitance permits only the long-term trends to be observed.

## ANALYSIS OF SPND SIGNAL CONDITIONING NETWORK

### Development of Transfer Functions

The input signal conditioning network for the SPND is shown in Figure 10. $Vout_1$ is the filtered output to the data system, and $Vout_2$ is the output to the multipoint recorder.

Since the network is passive, the loading effects of the SPND must be considered in order to develop transfer functions for $Vout_1$ and $Vout_2$. Figure 11 illustrates the lumped parameter electrical equivalent circuit for the SPND. Combining Figures 10 and 11 yields the network to be analyzed. The desired transfer functions are $Vout_1/In$ and $Vout_2/In$. The complete circuit is illustrated in Figure 12. Normal, typical values for the SPND electrical parameters were chosen to allow the analysis to be performed even though the previous sections show the parameters wide-ranging and unpredictable.

By comparing the time constants of $\tau_1 = C_c\ Req_1$ and $\tau_2 = C\ Req_2$, it becomes obvious that some simplifying assumptions can be made. $Req_1$ is the Thevenin resistance seen by capacitor $C_c$, assuming capacitor C is a short circuit. $Req_2$ is the Thevenin resistance seen by capacitor C, assuming capacitor $C_c$ is an open circuit.

$$Req_1 = 7.33\ K\Omega \tag{29}$$

$$Req_2 = 33.44\ K\Omega \tag{30}$$

$$\tau_1 = C_c\ Req_1 = 0.02 \times 10^{-6} \times 7.33 \times 10^{3} = 1.466 \times 10^{-4}\ s \tag{31}$$

$$\tau_2 = C\ Req_2 = 33.44 \times 10^{3} \times 120 \times 10^{-6} = 4.01\ s\ . \tag{32}$$

There are four orders of magnitude separating these two time constants; therefore, the capacitor $C_c$ will be neglected and replaced by an open

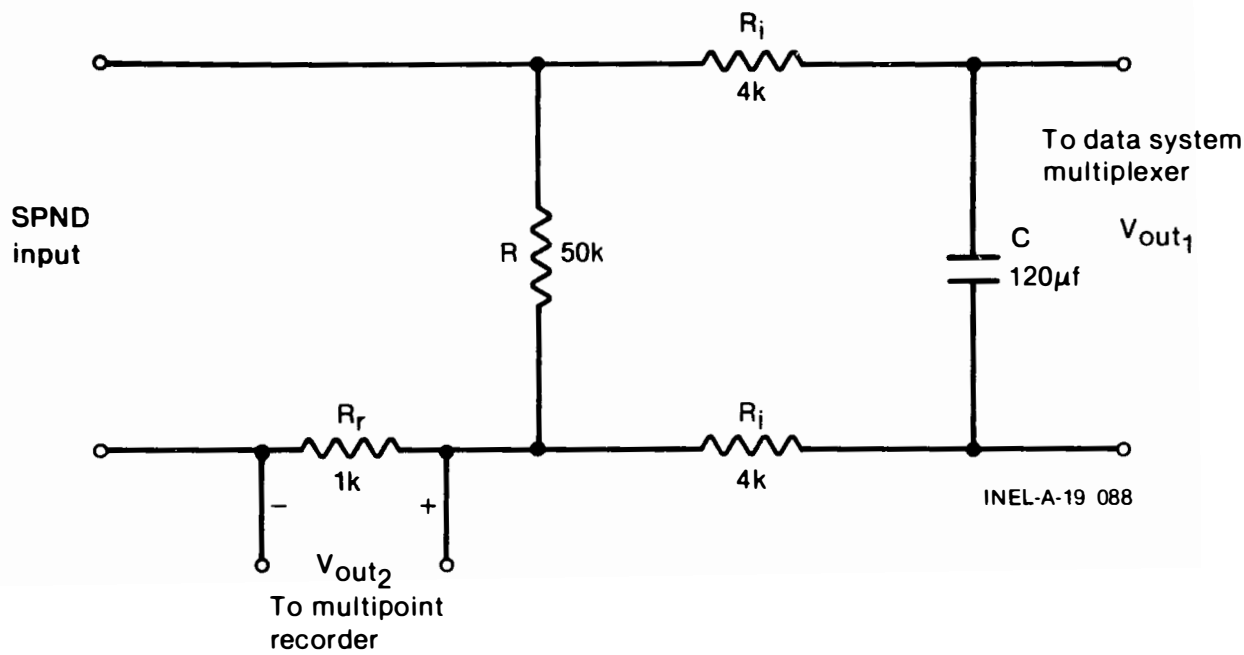


Figure 10. SPND signal conditioning network.

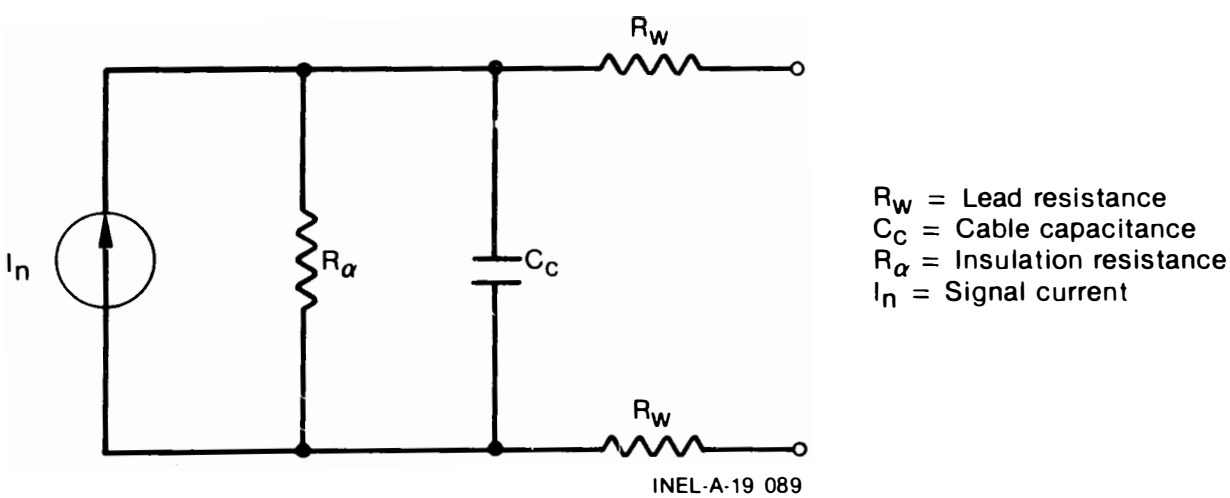


Figure 11. SPND equivalent circuit.

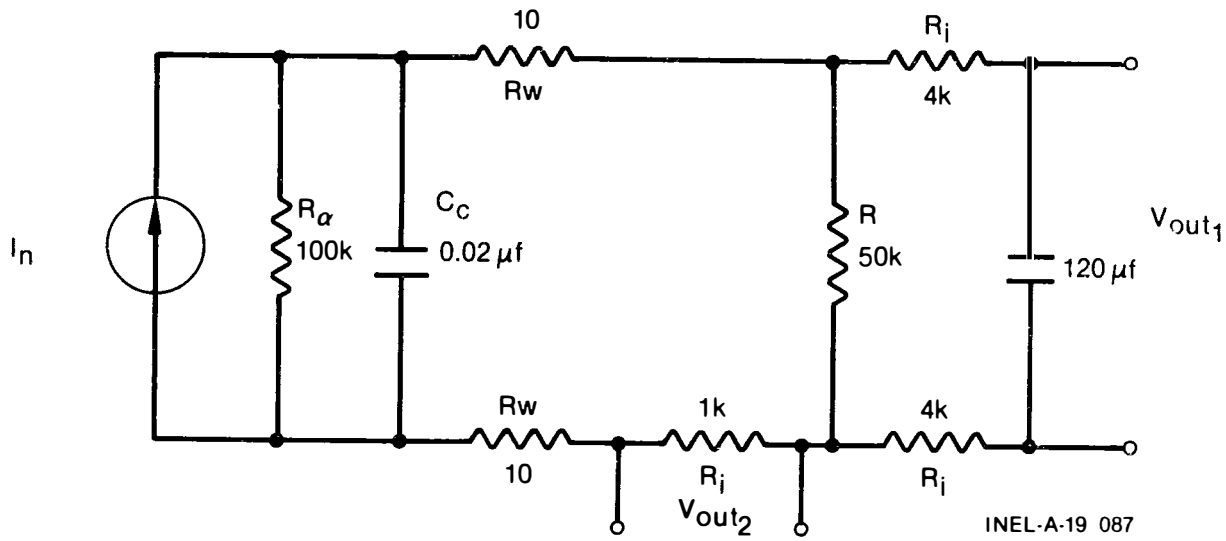


Figure 12. Complete SPND and signal conditioning network.

circuit. By similar reasoning, the lead resistance Rw will be neglected. The resultant simplified circuit is shown in Figure 13. The first transfer function to be developed is the output to the data system. Figure 13 can be simplified into Figure 14, where the current source and its source impedance are converted into its voltage source equivalent. The circuit of Figure 14 can be further simplified to the configuration of Figure 15, which is a passive, low-pass filter.

This is a first-order low pass with a 3db bandwidth of

$$f_c = \frac{1}{2\pi \; 2R_i + \left(\frac{R(R_\alpha + R_r)}{R + R_\alpha + R_r}\right)C} \tag{33}$$

The complete transfer function is

$$\frac{V_{out}}{I_{in}} = \frac{\frac{R_\alpha R}{R + R_\alpha + R_r}}{j\frac{f}{f_c} + 1} \quad . \tag{34}$$

Substituting in the following typical values

$R_\alpha$ = 100 KΩ

$R_r$ = 1 KΩ

R = 50 KΩ

$R_i$ = 4 KΩ

C = 120 μF

the transfer function becomes

$$\frac{V_{out1}}{I_n} = \frac{33.11 \text{ K}\Omega}{\frac{jf}{0.032} + 1} \tag{35}$$

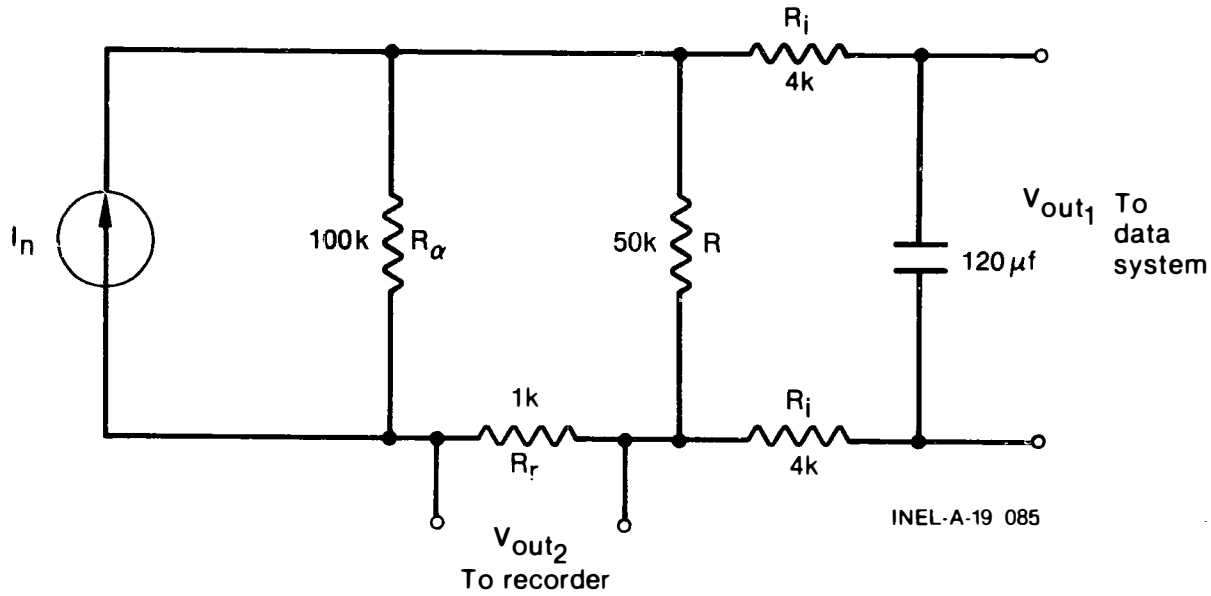


Figure 13. Simplified equivalent circuit.

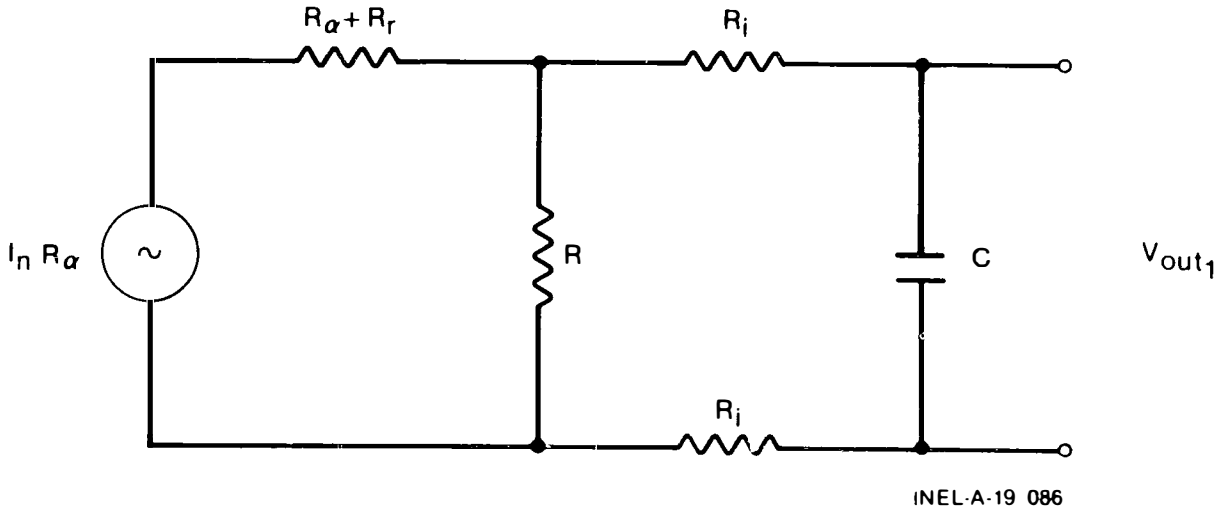


Figure 14. Equivalent circuit with voltage source excitation.

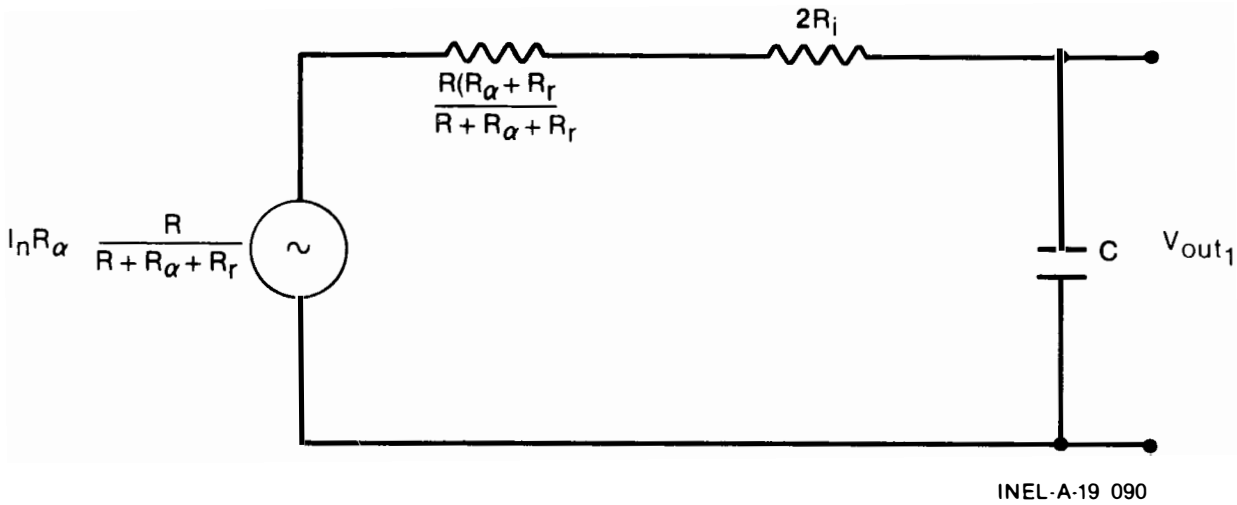


Figure 15. Equivalent circuit as a low-pass filter.

where f is frequency in Hz.

Returning to the simplified equivalent circuit of Figure 13, the transfer function for the multipoint recorder will be derived. Again, the circuit can be simplified using circuit theorems resulting in Figure 16: The transfer function $\frac{V_{out2}}{In}$ can now be easily derived:

$$\frac{V_{out2}}{I_n} = R_\alpha\left(\frac{R_r}{R_\alpha + R_r + Z}\right) \tag{36}$$

where

$$Z = \frac{\left(R\ 2R_i + \frac{R}{SC}\right)}{R + 2R_i + \frac{1}{SC}}$$

then

$$\frac{V_{out2}}{I_n} = \frac{R_r R_\alpha}{R_r + R_\alpha + R} \cdot \frac{\left[\frac{S}{\frac{1}{(R + 2R_i)C}} + 1\right]}{\left\{\frac{S}{\frac{1}{\left[\frac{(R + 2R_i)(R_\alpha + R_r) + 2R_i R}{R_\alpha + R_r + R}\right] C}}\right\} + 1} \tag{37}$$

Substituting s = j2πf and the following typical values

$R = 50\ K\Omega$

$R_\alpha = 100\ K\Omega$

$R_r = 1\ K\Omega$

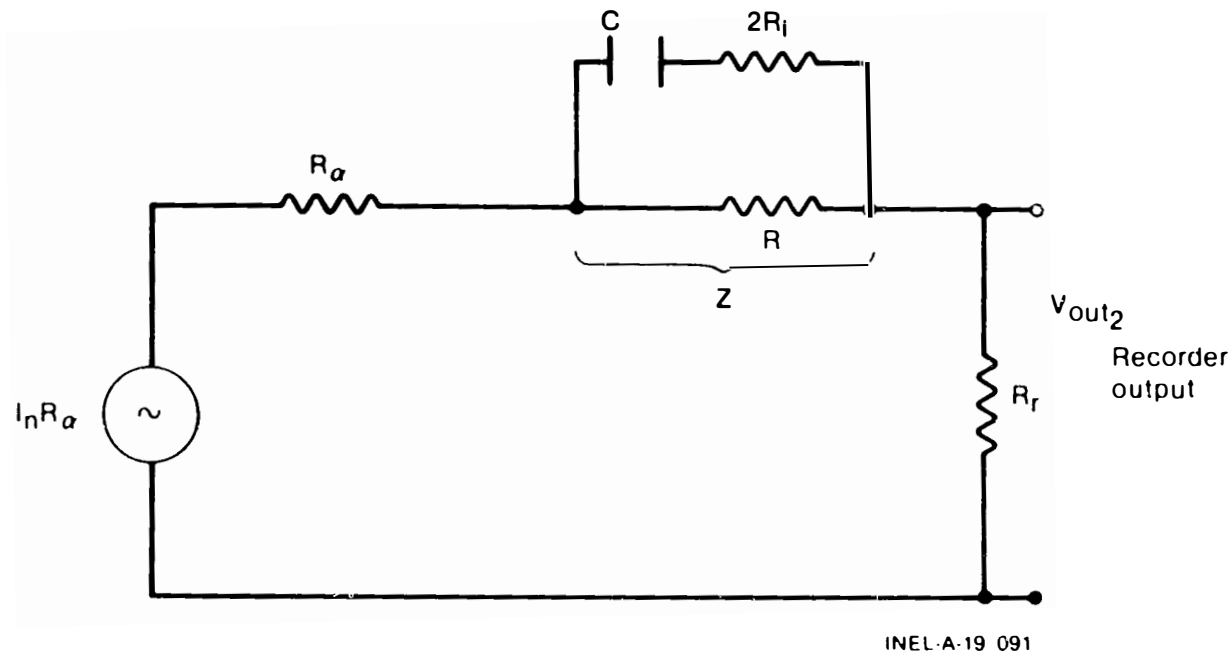


Figure 16. Resultant recorder equivalent circuit.

$R_i$ = 4 KΩ

C = 120 μF

the transfer function becomes

$$\frac{V_{out2}}{I_n} = 662.25\left(\frac{\frac{jf}{0.02286} + 1}{\frac{jf}{0.0320} + 1}\right) \tag{38}$$

where f = frequency in Hz at DC, $V_{out2}/I_{IN}$ = 662.25Ω. At frequencies above 0.1 Hz, $V_{out2}/I_{IN}$ = 927Ω. Figure 17 illustrates a plot of the transfer function for the recorder output. This output is not filtered. In actuality, some filtering would be provided by the parasitic cable capacitance $C_c$, shown in Figure 12. However, the cutoff frequency would be at about 1 kHz. This output is virtually unfiltered relative to the recorder sample frequency of every 2.5 min.

## The Aliasing Problem

### Theoretical Background

Whenever an analog system signal is sampled at a frequency $f_s$, all the signal power above the Nyquest frequency appears in the sample spectrum below the Nyquest frequency as noise. The Nyquest frequency is half the sample frequency:

$$f_n = \frac{f_s}{2} \tag{39}$$

where

$f_n$ = Nyquest frequency

$f_s$ = sample frequency.

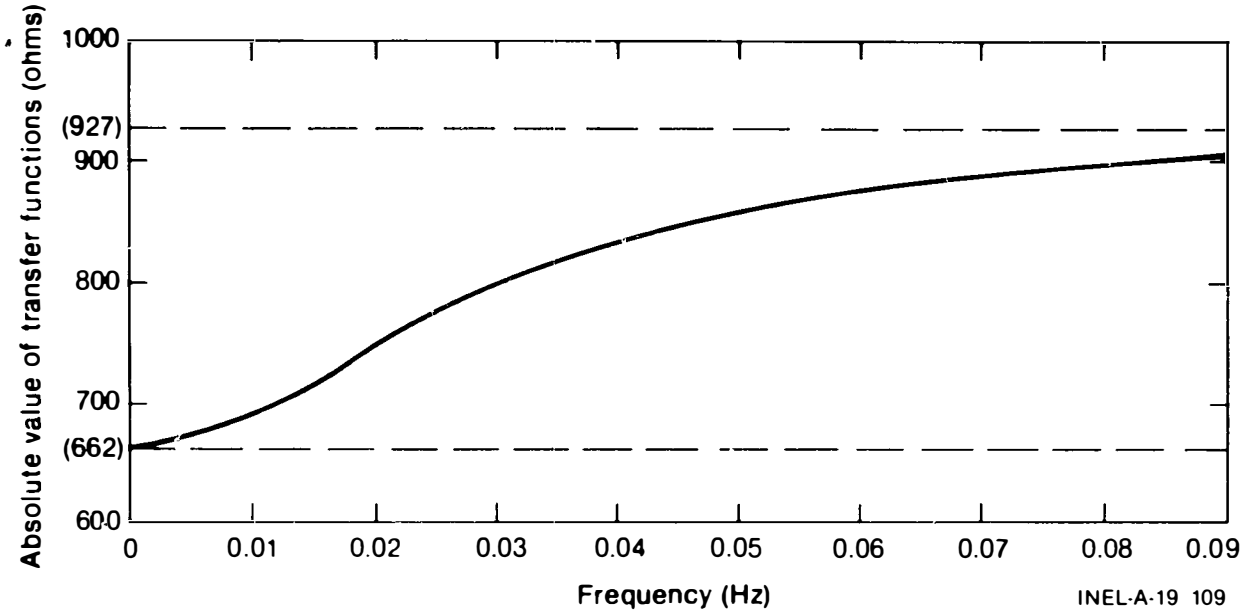


Figure 17. Plot of recorder transfer function.

Suppose the signal has a power density spectrum $p(w)$ where $w = \frac{f}{f_c}$ and where $f$ = frequency; $f_c$ = cutoff frequency.

The total signal power is $\int_0^\infty p(w)\, dw$.

For a signal sampled at $f_s$ or $w_s = \frac{f_s}{f_c}$, the sampled signal power will be

$$S^2 = \int_0^{w_n} p(w)\, dw \tag{40}$$

where

$$w_n = w_s/2.$$

The noise from aliasing will be all the power above $w_n$, and is given by

$$n^2 = \int_{w_n}^{\infty} p(w)\, dw\ . \tag{41}$$

Thus, the signal-to-noise power for the sampled signal becomes

$$\frac{S^2}{N^2} = \frac{\int_0^{wn} p(w)dw}{\int_{w_n}^{\infty} p(w)dw}\ . \tag{42}$$

For the data system the input filter is a first-order low pass. If the input signal is assumed to be much wider bandwidth than the input filter, then the spectrum becomes that of the input filter. The power density of a magnitude and frequency normalized first-order system is given by

$$p(w) = \frac{1}{w^2 + 1} \tag{43}$$

where

$$w = \frac{f}{f_c}$$

where

$f$ = frequency

$f_c$ = 3db cutoff frequency.

See circuit sketch, Figure 18.

The signal power is

$$\int_0^{\infty} p(w)dw = \int_0^{\infty} \frac{1}{w^2 + 1} dw = \pi/2 \ . \tag{44}$$

The sampled signal power is

$$S^2 = \int_0^{wn} p(w)dw \tag{45}$$

$$S^2 = \int_0^{wn} \frac{1}{w^2 + 1} dw = \mathrm{Tan}^{-1} w \Big|_0^{wn} \tag{46}$$

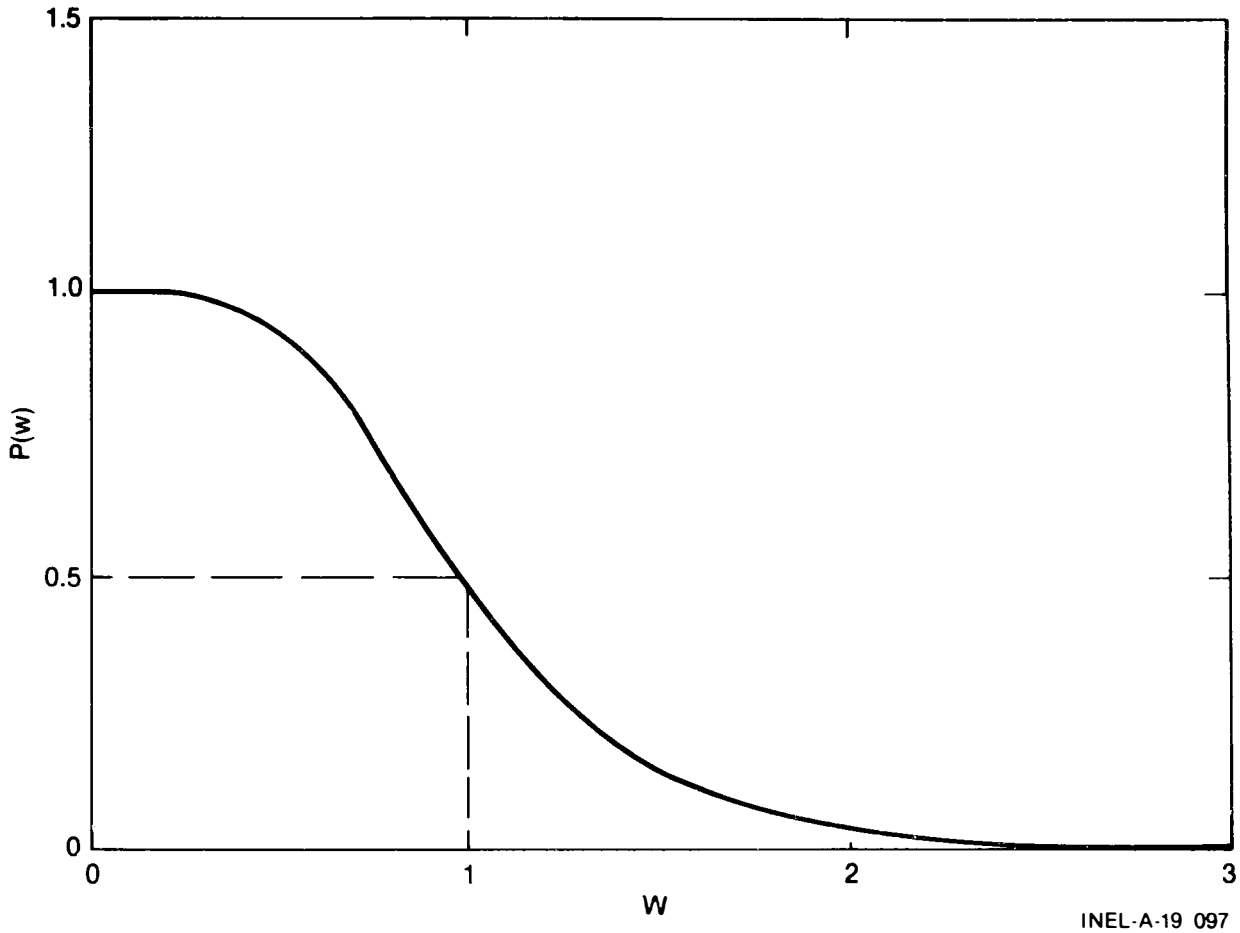


Figure 18. Sketch of P(w) for first-order low-pass.

$$S^2 = \mathrm{Tan}^{-1}\, wn = \mathrm{Tan}^{-1} \frac{f_s}{2f_c} . \tag{47}$$

The aliased power is

$$N^2 = \int_{wn}^{\infty} p(w)dw = \int_{wn}^{\infty} \frac{1}{w^2 + 1} dw = \mathrm{Tan}^{-1}\, w \Big|_{wn}^{\infty} \tag{48}$$

$$N^2 = \pi/2 - \mathrm{Tan}^{-1}\, w_n = \pi/2 - \mathrm{Tan}^{-1} \frac{f_s}{2f_c} . \tag{49}$$

Thus, for a normalized first-order system the signal-to-aliased noise ratio is

$$\frac{S^2}{N^2} = \frac{\int_0^{wn} p(w)dw}{\int_{wn}^{\infty} p(w)dw} = \frac{\mathrm{Tan}^{-1} \frac{f_s}{2f_c}}{\pi/2 - \mathrm{Tan}^{-1} \frac{f_s}{2f_c}} . \tag{50}$$

Figure 19 gives $S^2/N^2$ plotted against $f_s/f_c$ for a first-order system.

In order to provide some physical meaning to all the mathematics, graphical illustrations were prepared. The power density spectrum for the first-order system is carefully plotted in Figure 20. This figure is a plot of the sketch illustrated in Figure 18. The shaded area under this curve represents the total unsampled signal power. Two cases are illustrated in additional figures. The first case is where the sampling frequency is at just twice the cutoff frequency. For this case, the Nyquest frequency is given by

$$f_n = \frac{f_s}{2} = \frac{2f_c}{2} = f_c \tag{51}$$

for sampling at twice the cutoff frequency.

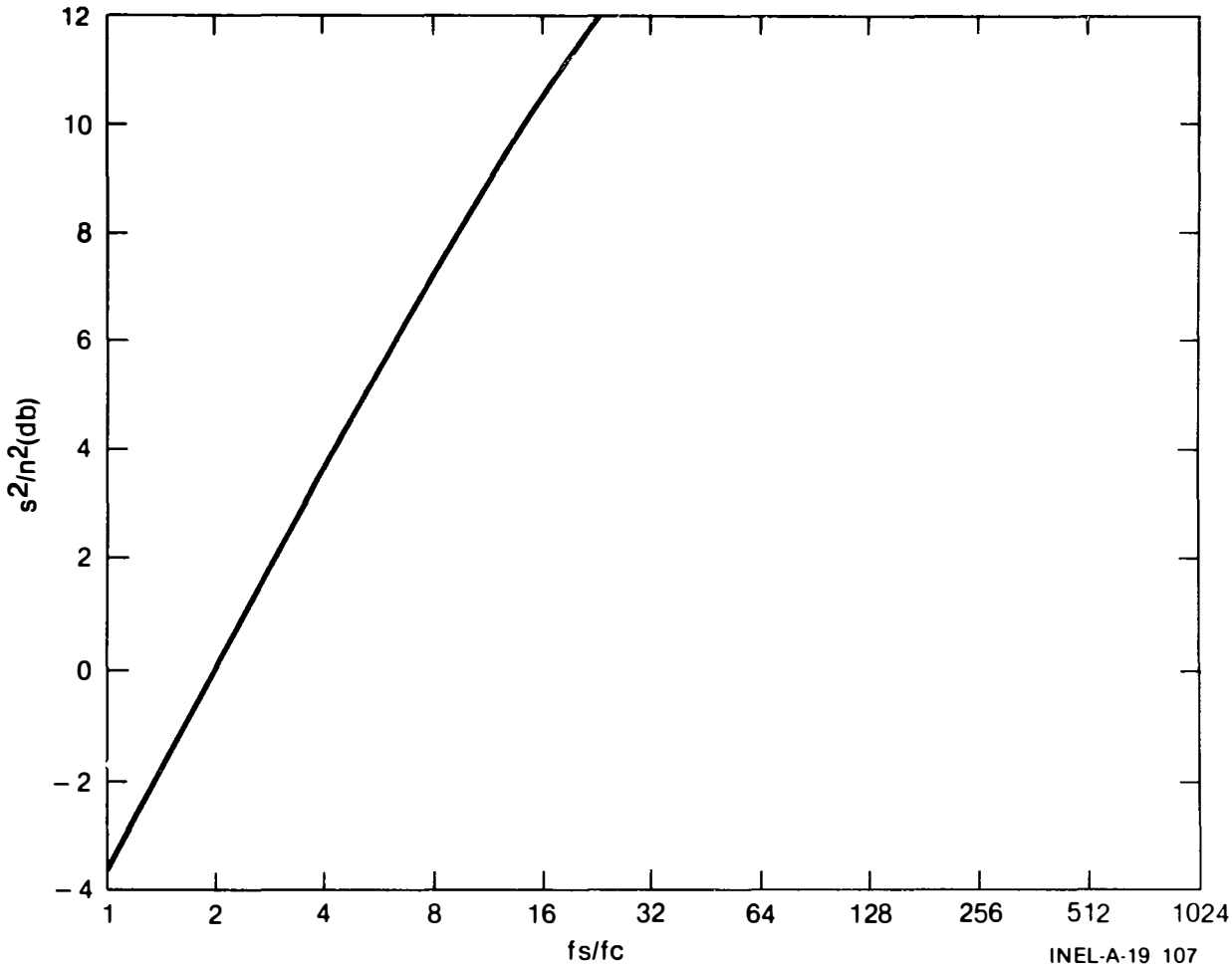


Figure 19. Signal-to-noise power ratio vs. sample-frequency-to-cutoff-frequency ratio for a first-order system.

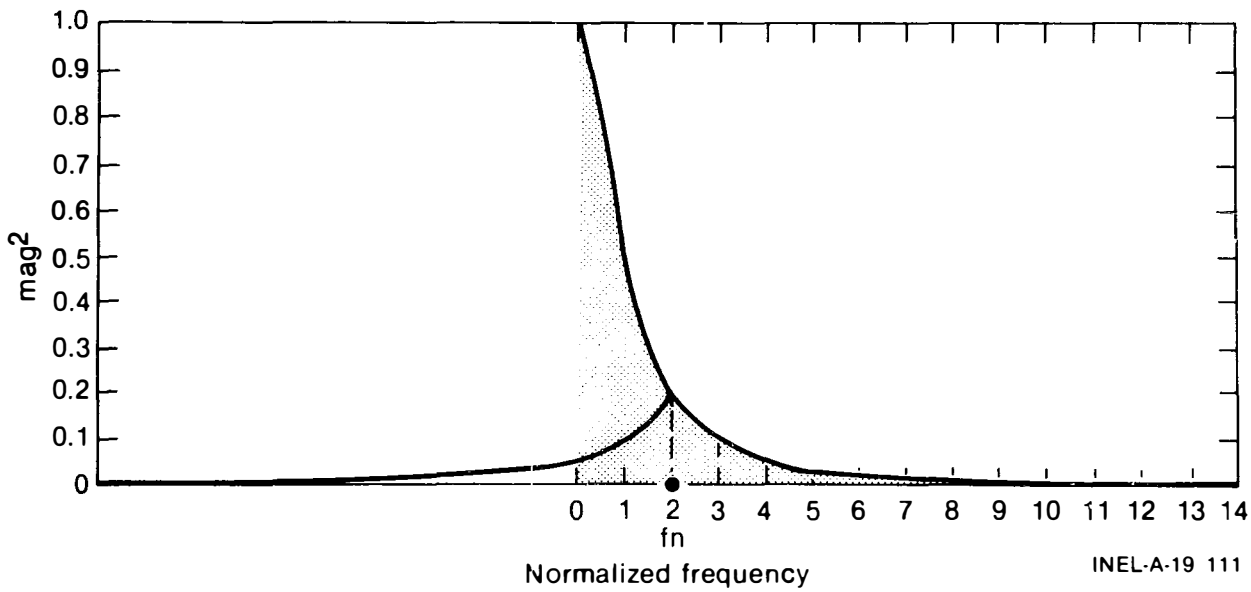


Figure 20. Total signal power prior to sampling.

The sampled signal power is shown by the shaded area in Figure 21. The aliased power is shown by the shaded area in Figure 22. For the first case, the two areas are equal and the $S^2/N^2$ is 0 db.

The second case illustrated is where the sampling frequency is four times the cutoff frequency. For this case the Nyquest frequency is given by

$$f_n = \frac{f_s}{2} = \frac{4f_c}{2} = 2f_c \tag{52}$$

for sampling at four times the cutoff.

The sampled power is shown by the shaded area in Figure 23. The aliased power is shown folded back and shaded by Figure 24. For this case, the $S^2/N^2$ = 3.78 db, which is not really adequate.

Extent of the Aliasing Problem for the SPND During the Accident

The SPND signal into the recorder shown by the analysis and sketched in Figure 10 is not bandwidth limited until about 1 Hz. The mechanical drive of the recorder offers the only real bandwidth limiting. If the recorder bandwidth is assumed to be 1 Hz, and an input of white noise is considered, then with the recorder sample rate of 1.5 min/sample, the aliasing problem is seen to be immense. Calculating the signal-to-noise ratio,

$$\frac{S^2}{N^2} = \frac{\mathrm{Tan}^{-1}\frac{f_s}{f_c}}{\pi/2 - \mathrm{Tan}^{-1}\frac{f_s}{f_c}} \tag{53}$$

$$\frac{S^2}{N^2} = 4.26 \times 10^{-3} = -23.6 \text{ db} \tag{54}$$

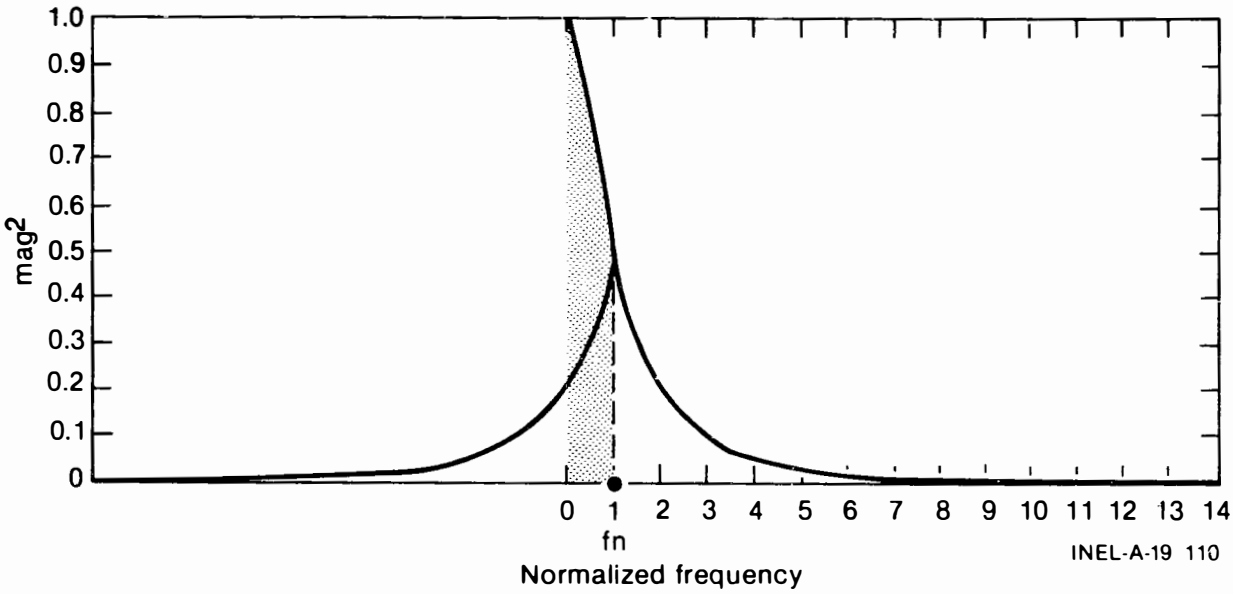


Figure 21. Sampled signal power; Case 1--fs = 2 fc.

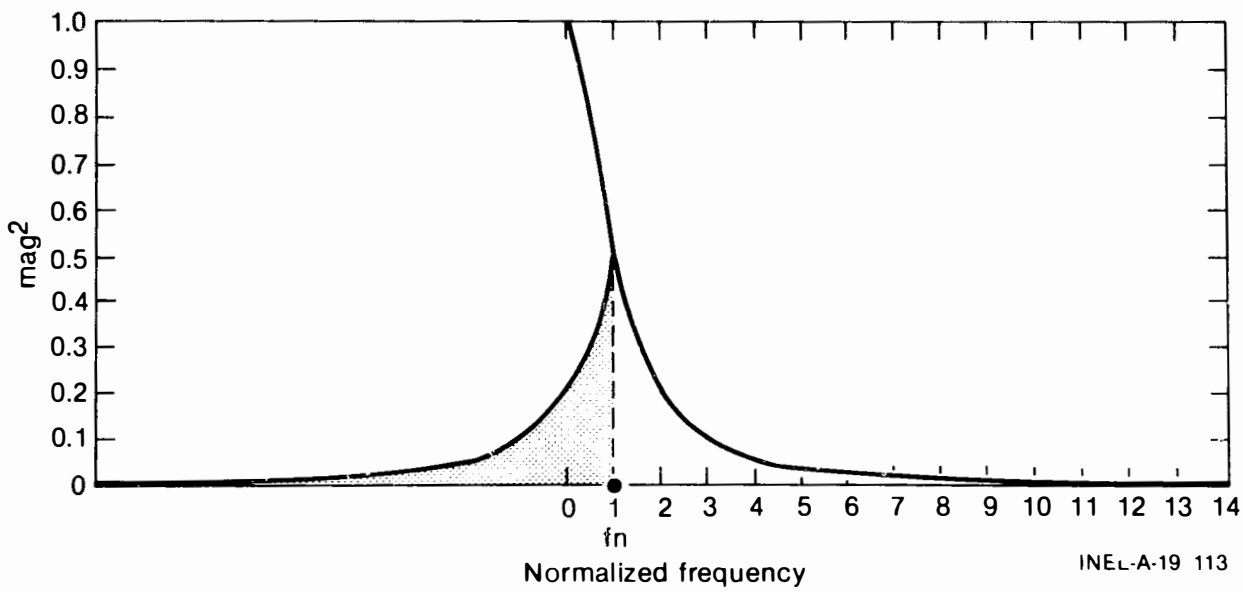


Figure 22. Total aliased power; Case 1--fs = 2 fc.

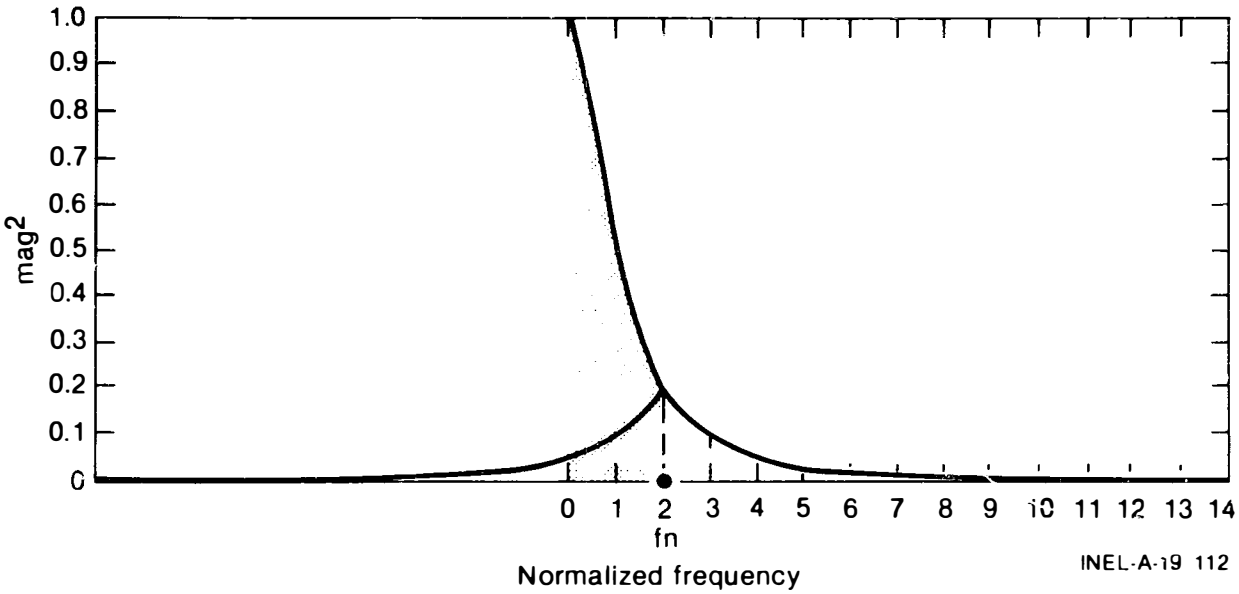


Figure 23. Sampled signal power; Case 2--fs = 4 fc.

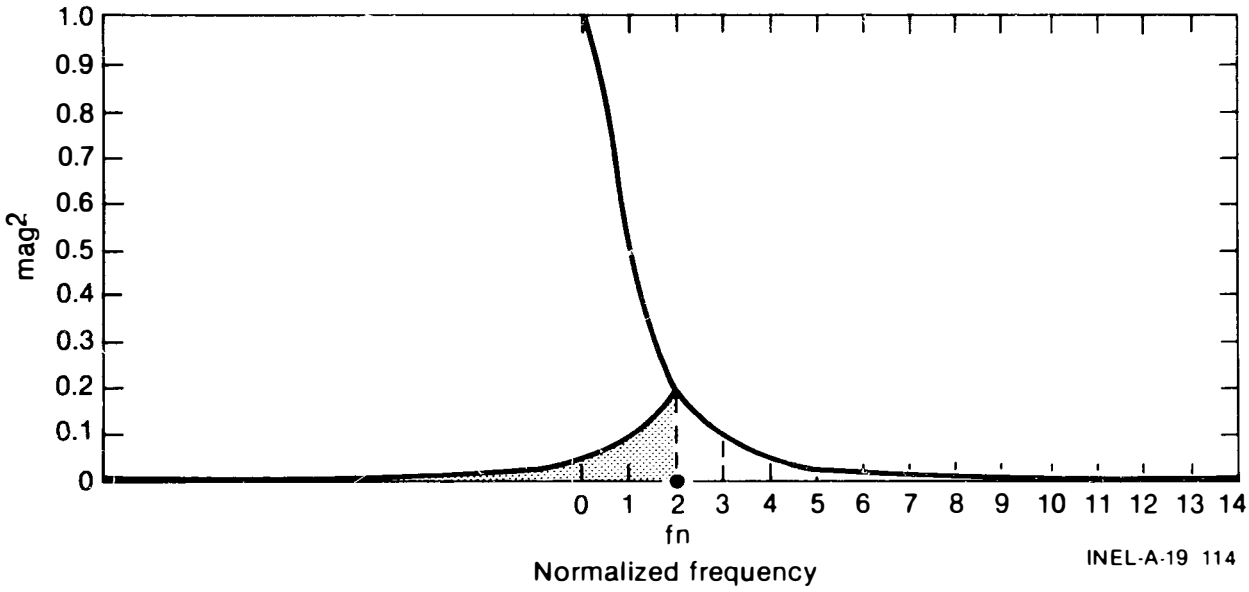


Figure 24. Total aliased powr, Case 2--fs = 4 fc.

where

$$f_c = 1 \text{ Hz}$$

$$f_s = \frac{1}{2.5 \times 60} = 6.67 \times 10^{-3} \text{ Hz}.$$

Basically, this says that unless one can imagine some bandwidth limiting in the signal by something other than the recorder that is significantly more limiting than $6.67 \times 10^{-3}$ Hz, then the recorder data for the SPNDs as observed is very badly contaminated with aliasing noise. This is particularly true during the time of core damage, since it seems reasonable to assume that while that coolant was boiling, temperature excursions were happening faster than every 2.5 min.

Aliasing in the data system SPND channels is a similar problem. From the input filter transfer function analysis, the cutoff frequency was shown to be 0.032 Hz with a first-order low pass. For the SPND channels in the data system, the sample frequency is 15 s. This is

$$f_s = 0.0666 \text{ Hz} \tag{55}$$

and

$$\frac{f_s}{f_c} = \frac{0.0666 \text{ Hz}}{0.032 \text{ Hz}} \cong 2 \quad . \tag{56}$$

From Figure 19, it can be seen that $S^2/N^2$ for $f_s/f_c = 2$ is only 0db. This is exactly the case illustrated by Figures 21 and 22. Even with $S^2/N^2 = 0$ db, the uncertainty in the data is so high that the information is lost. As with the recorder, unless one can imagine some other bandwidth limiting in the signal besides the input filter, it can be concluded that the signal-to-noise ratio of 0 db for the SPND data channels is a fact.

## Extent of the Aliasing During Normal Operation

It must not be concluded from this report that our purpose is to detail design deficiencies of the SPND measurement system. Rather, our purpose is to show that the SPND measurement system designed o measure steady state neutron flux distribution in the reactor core will not provide any meaningful data when it is used to measure the transient temperature excursions that occurred during the accident. It has been shown by analysis that wide bandwidth signals that are input into this measurement system will result in an output that is severely distorted with aliasing noise. However, if the signal is bandwidth limited, as the neutron flux associated with steady state reactor power most likely is, then the aliasing noise associated with this measurement system, when used as it was intended, is not a problem.

## Conclusions and Recommendations

Obviously, the main conclusion of this report is that this SPND measurement system cannot be used to quantitatively measure temperature in the core during the accident. A recommendation is that the various measurement channels be reviewed from a systems point of view to determine if aliasing was adequately addressed during the design. If this problem was not addressed, it is recommended that tests and analyses be performed to try to determine the extent of the problem.

## CONCLUSIONS

All parts of this report have attempted to bound the characteristics of each block in the measurement system diagram of Figure 2 (repeated below). Table 11 summarizes these characteristics.

TABLE 11. SUMMARY OF MEASUREMENT SYSTEM CHARACTERISTICS

| BLOCK | SUMMARY |
|---|---|
| Heat transfer characteristics, fuel rod to SPND | A gain factor with a variation of up to 40 to 1, conservatively |
| SPND temperature response | It has a fairly predictable temperature response over the range of interest. However, the temperature is not only from convection of radiation from fuel,but from self-heating by the gamma flux. |
| Cable response | Over the temperature range of interest, it introduces a noise signal that is a function of gamma heating, integrated temperature over the length of the cable, and how fast the water level is decreasing in the core. It also causes widely varying signal dynamics due to temperature effects on insulation resistance and cable capacitance. |
| Data system | Worst-case signal-to-noise ratio from aliasing is 0db |
| Recorder system | Worst-case signal-to-noise ration from aliasing is -24db |

Examining Table 11, it is apparent that any information from the recorder or data system cannot be converted into fuel temperature. It should be noted, however, that the aliasing problem of the recorder system and data system is mitigated when the cable response and SPND response starts degrading due to the high time constants introduced.

## REFERENCES


1. Frank Kreith, Principles of Heat Transfer, 3rd edition, New York: Intext Educations Publishers, 1973.

2. J. P. Holman, Heat Transfer, 2nd edition, McGraw-Hill.

3. Orvid W. Eshbach, Handbook of Engineering Fundamentals, 3rd edition: John Wiley, 1975.

4. D. M. Peterson, G. A. Graves, and R. L. Seale, "Studies of $U^{235}$ Post Fission Gamma and Beta Radiation and of Post-Shutdown Radiation Release from Fission Operations at Constant Power," LA-2903, 1964.

5. Ned Wilde, "Analysis of an Analog-to-Digital Conversion System," EG&G Idaho, Inc., internal report.

6. Samuel D. Stearns, "Digital Signal Analysis," Rochelle Park, New Jersey: Hayden Book Company, 1975.

# APPENDIX A

# SPWD PRODUCT SPECIFICATION

| Belfab<br>Bailey Babcock & Wilcox | Product Specification<br>M203 |
|---|---|

# SELF POWERED NEUTRON DETECTORS

**An incore detector that provides a current output proportional to the thermal neutron flux density of the reactor core, with no external power source required.**

## Application

For use under any of the following conditions:

- For multiple fixed location continuous monitoring.
- For moveable single non-continuous monitoring of any point in the core.
- For both fixed and moveable monitoring combined.
- Incore assemblies supplied with either solid or flexible oversheath for use in either top or bottom entry cores.

## Features

- Swaged construction gives over 95% compaction of insulation allowing greater than $10^{13}$ ohms insulation resistance at room temperature.
- Solid oversheath allows unit to be exposed directly to coolant pressure and temperature.
- Multiple detectors in each assembly allow readings along entire core length.
- Background detector gives average or reference reading to compensate for induced leadwire signal.
- Various types of background units are available, e.g., single lead - Inconel or Zircalloy 2 or twinlead.
- Center tube provided for calibration probe or moveable self-powered detector to monitor any core location.
- Thermocouple(s) provide inlet and/or outlet temperature reading.
- With solid oversheath and center tube typical unit will bend easily on a four (4) foot (1.219m) radius.
- Outersheath and detector sheaths pressure tested at 4,000 psi (27,580 kPa).
- With flexible (non-solid) sheath, bend radius of less than one (1) foot (.305m) is attainable.
- Assemblies can utilize various combinations of materials and components.

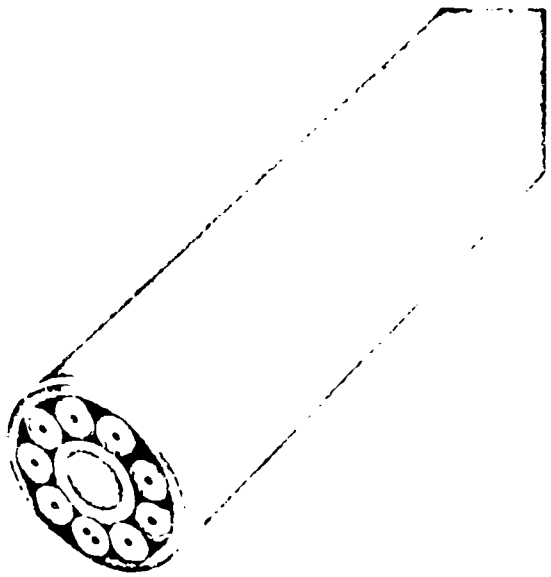

Cross Section of Typical Incore Detector Assembly

## Typical Incore Detector Assembly

- Length 35 to 130 feet (10.668 to 39.623m).
- Outer diameter .300 inches (7.62mm) nominal.
- 7 individual flux detectors
- 1 background detector
- 1 thermocouple
- 1 center tube
- 1 high pressure oversheath
- 1 high pressure closure housing
- 1 multiconductor electrical connector

# M203 Self Powered Neutron Detectors

## Assembly Materials

Oversheath and detector sheath

- Inconel 600
- 300 Series Stainless Steel

Leadwire

- Inconel 600
- Dilvallay 3

Insulation

- Magnesium Oxide
- Aluminum Oxide

Emitter

- Rhodium
- Vanadium
- Gadolinium
- Ytterbium

Connectors

- As required to match interconnect cable

Belfab can also supply interconnect cable and drive units for moveable units.

To receive a quotation please contact Belfab Sales Department to discuss your application.

Sales Department
Belfab, Bailey Controls Company
P. O. Box 9370
Daytona Beach, Florida 32020

# APPENDIX B

# THE DESIGN OF A SPND ELECTRICAL SIMULATOR FOR 1200 TO 1800°F REGION

Babcock & Wilcox

Power Generation Group

P.O. Box 1260, Lynchburg, Va. 24505
Telephone: (804) 384-5111

BW/GPU-80-194

November 11, 1980

Mr. G. K. Hovey
GPU Service Corporation
P.O. Box 480
Middletown, PA 17057

Attention: Messrs. H. P. Wood (Bechtel)
R. Jacobstein (GPU)

Subject: Task 50-06, Evaluation of SPND Data
Simulator Circuit Diagrams

Reference: L. H. Lilien to G. E. Kulynych, Design and Fabrication of Self-Powered Neutron Detector Signal Simulator Control Instrument, (C-0338) dated August 14, 1980

Gentlemen:

Attached for your information and review, are draft schematic and block diagrams of the SPND Signal Simulator ("Black Box") and general discussion of the system design criteria. These are submitted for EG&G TIO review in accordance with the referenced authorization letter.

Components and materials for fabrication of the simulator have been placed on order and most have been received ahead of the expected delivery dates. Fabrication could begin at any time at the direction of GPU. Approximately one man-week of effort will be required to fabricate the simulator described herein.

Please be advised that approximately 85% of the allocated funds have been expended or committed on this task as of this date. No further work will be performed until we have received authorization to proceed with fabrication following the EG&G review of the attached diagrams. Your immediate attention to this review is requested in order that the task be completed in a timely manner.

Also please be advised that Mr. R.F. Ryan has assumed management responsibilities for this task. All technical matters should be directed to him and contractual matters directed to Mr. Kulynych.

If you have questions or comments or if we may be of further assistance, please advise.

Very truly yours,

THE BABCOCK & WILCOX COMPANY

G. E. Kulynych
TMI-2 Recovery Program Manager
by

D. G. Culberson
TMI-2 Service/Contract Manager

GEK/DGC:pbv
Attachment
cc: R.F. Wilson
J.J. Barton
J.C. DeVine
D.W. Demers
M.K. Pastor
R.L. Rider
J.W. Mock
L.H. Lilien
L.C. Rogers
G.T. Fairburn
File: 03-05-050-06

## APPENDIX B

## THE DESIGN OF A SPND ELECTRICAL SIMULATOR FOR 1200 to 1800°F REGION

To simulate the output of a self-powered nuclear detector (SPND) when in an environment like the reactor during the TMI-2 accident, one should consider two major parts.

First, it must be possible to simulate the temperature profile versus time that the detector would see. It has previously been shown that neutron activity was not a major factor in the environment for the SPND after the initial few minutes of the accident and, therefore, temperature is the major input to the detector. This profile included both long-term trends giving gross effects and rather rapid changes that would be expected when the SPNDs were partially uncovered, heated by the fuel, then splashed with much cooler water from the pot boiling activity below

The second major part is the characteristics of the SPND over the temperature range anticipated. Four major characteristics have been observed or hypothesized. These are leakage resistance change, thermionic current, dielectric thermal relaxation charge, and capacitance (dielectric constant change versus temperature).

The thermionic current characteristics of Belfab, Bailey Controls Company SPND is well documented in a report to EPRI by H. D. Warren, LR:79:4817-01:1, dated July 30, 1979. A reasonable fit to this data in the 1200 to 1800°F region is given by

$$i_H = -1 \times 10^{-8} \times e^{(T - 1200) \times 0.01334}$$

where

$i_H$ = thermionic current in amps

$T$ = temperature in °F.

The influence of radiation on this thermionic current is small and has been reported by H. D. Warren and M. N. Baldwin to EPRI Technical Service Agreement 79-307.

The leakage resistance of SPNDs has been measured by R. C. Roberts and H. D. Warren. There is some influence of past history of the detector on this characteristic. Of particular importance is previous heating. Since the TMI detectors had been annealed at about 1600°F, data from an annealed detector was used. A good fit of the data for detectors of similar construction heated only in the incore 12 ft of length is

$$R = 3 \times 10^{6} \times e^{-(T - 1200°F) \times 0.01367}$$

where

R = leakage resistance in Ω

T = temperature in °F

in the 1200 to 1800°F region.

Two additional characteristics have been noticed during testing at higher temperatures. First is very large changes in capacitance of the detector assembly. At room temperature, the capacitance is about 96 pF/ft. Considering the geometry of the detector, the effective dielectric constant is about 7.68. After applying a voltage to measure resistance at 1600°F, it was noticed that a very long discharge period was required. This proved to be because of very large stored energy or high capacitance. The capacitance had increased from 96 pF/ft to 83 mFd/ft. This would require an effective dielectric constant of $8 \times 10^{5}$. Although no specific measurement results were found in a literature review, all indications are that above 700°F the dielectric constant goes up very rapidly and that constants of $10^{5}$ are very likely at 1600°F and DC. (Note: the AC resistance is well documented and is very much lower at high frequency). Other measurements at B&W's Lynchburg Research Center confirmed this very large change in capacitance at temperatures above 700°F.

Dielectric absorption, the slow release of retained charge over time, and dielectric thermal relaxation (the release of retained charge by raising the temperature) are also seen. The dielectric thermal relaxation seems to be of major significance. Charge locked in the dielectric ($Al_2O_3$) is released at temperatures of 1300 to 1800°F. This charge has been measured to be between $10^{-3}$ and $10^{-2}$ coulombs for 12 ft of detector. This charge produces a positive current. When only a part of a detector is subjected to high temperature only the charge of this portion of the detector is released. The total charge in a section is released in tens of seconds when heated rapidly. This can happen only one time for any portion of a detector, for once the charge is released no recharging mechanism exists.

If the portion of detector exposed to high temperatures moved down as the water boiled out of the core, the thermal relaxation current would be either continuous or pulsating depending on the temperature profile seen. This current is a function of temperature, time and past history. The thermionic current and the leakage resistance would change with time but would fluctuate somewhat less since they are the integrated effect over the total length and a function temperature alone.

A block diagram of the incore simulator is shown in Figure B-1. Each of the major sections is in blocks. They are:

1. TEMPERATURE TREND PROGRAMMER--Produces the long-term trend or profile of temperature. It works by forcing the beam of a CRT, HP 1340A, to trace the edge of a shadow mask program. The ramp generator allows this program to run at a 3 minute to 2 hour per sweep. The shadow mask will allow programming any temperature profile in the 1200 to 1600°F range. Since it operates in the analog domain, the output is continuous with an accuracy of about 3% of full scale.

2. TEMPERATURE FLUCTUATION PROGRAMMER--Used to produce rapid fluctuation of temperature with respect to time. It consists of an HP 3310A Function Generator. This signal is added to the temperature trend signal.

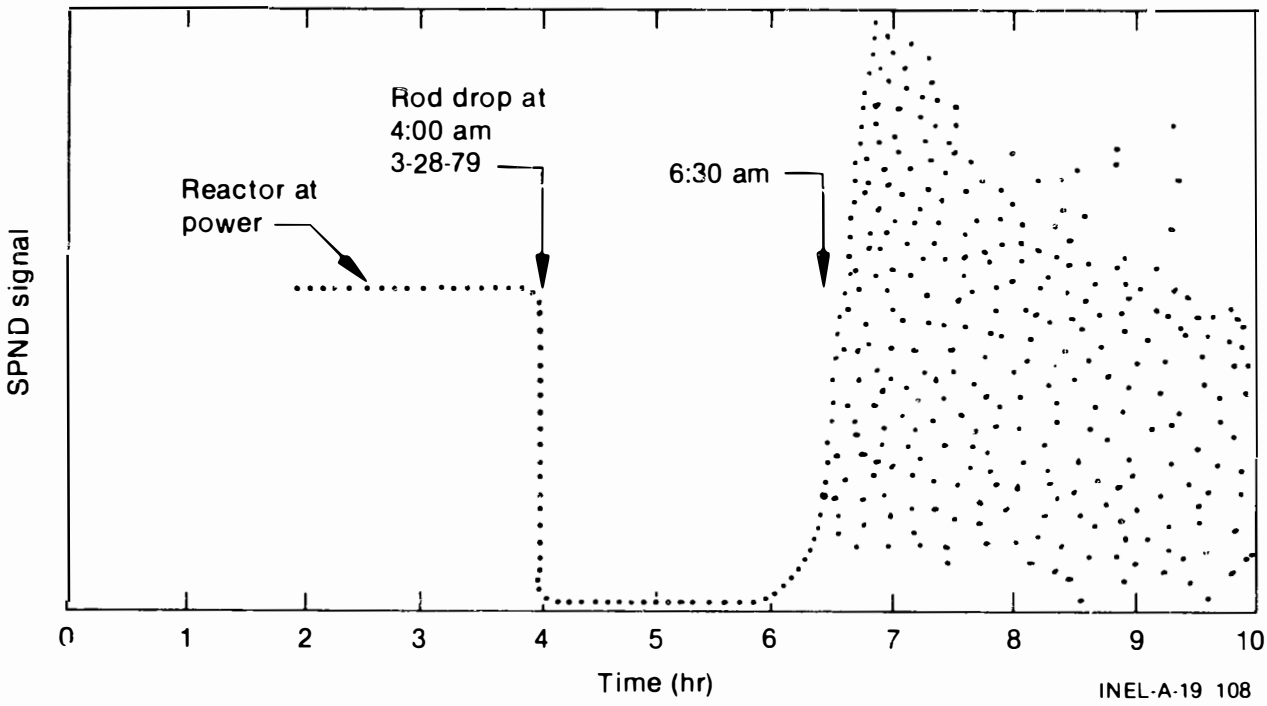


Figure B-1. Backup recorder's tracing of in-core detector signals.

3. LEAKAGE RESISTANCE FUNCTION GENERATOR--R = f(T); produces an electrically isolated resistance.

$$R = 3 \times 10^{6} \times e^{-(T-1200°F)} \times 0.01367$$

4. THERMIONIC FUNCTION GENERATOR--$I_T$ = f(T); produces an output current

$$I_T = -10^{-8} \times e^{(T-1200)} \times 0.01334$$

This current source has a voltage compliance of $\pm$ 10 VDC.

5. DIELECTRIC THERMAL RELAXATION CHARGE FUNCTION GENERATOR--$I_D$ = f(T,t). It was assumed that, on the average, water boiled down in the core as a linear function of time. Therefore, charge available for thermal relaxation is directly proportional to time. The available charge is released as a function of temperature and with a shaping filter to produce an attack and decay time (10 sec and 50 sec respectively) to match those measured in the lab. The charge available accumulates at an adjustable rate from $30 \times 10^{-9}$ to $300 \times 10^{-9}$ coulombs/sec. The output is a current source which has a voltage compliance of $\pm$ 10 VDC.

6. DETECTOR CAPACITANCE--C. Little is known about the dynamic characteristics of this change and the simulator simply has a selector switch to choose a fixed C that is independent of temperature.

A schematic diagram of the "Black Box" portion to be constructed is shown in Figure B-2. This box will interface to other B&W-supplied general purpose test equipment. To associate the segments of the schematic associated with each of the blocks previously described, see Table B-1.

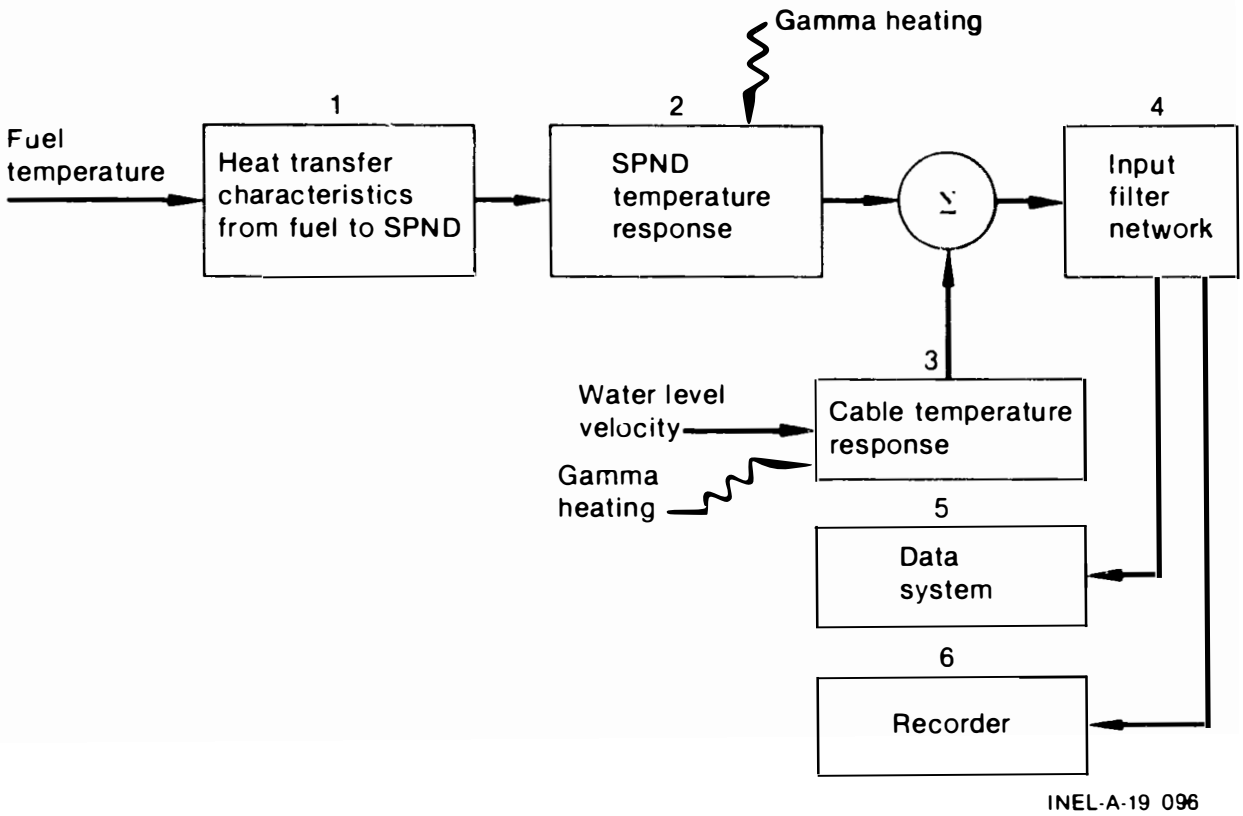


Figure B-2. Block diagram of SPND measurement system for measuring fuel rod temperature.

TABLE B-1. SCHEMATIC DIAGRAM GIUDE FOR IN-CORE SIMULATOR

| Block Description | Schematic Area | Output |
|---|---|---|
| Temperature trend programmer | 11 to 17 x A to G | 14F |
| Temperature fluctuation programmer | 12 to 16 x H to I | 13H |
| Leakage resistance function | 1 to 10 x A to C | 1C |
| Thermionic function generator | 1 to 10 x D to F | 3E |
| Dielectric thermal relaxation | 1 to 10 x G to J | 3H |
| Detector capacitance | 1 to 3 x J to K | 2J |

The switches used to control the device are described in Table B-2.

TABLE B-2. IN-CORE SIMULATOR CONTROL SWITCHES

| | |
|---|---|
| SW 1 | Holds the output of the temperature programmer at 1200°F |
| SW 2 | Resets and holds time at "0" for the temperature programmer |
| SW 3 | Resets dielectric thermal relaxation temperature peak detector |
| SW 4 | Resets dielectric thermal relaxation charge available to zero |
| SW 5 | Isolates resistance characteristic section |
| SW 6 | Isolates thermionic current section |
| SW 7 | Isolates dielectric thermal relaxation section |
| SW 8 | Isolates cable/detector capacitance section |

A meter will show average temperature in order to follow the progress of a test during normal operation. It will show 1200 to 1800°F.

All of the parts of the simulator will be assembled in a general purpose equipment enclosure and should be quite portable. Only the ramp adjustment, sweep speed, the switches and the meter are front panel mounted. Numerous "trim pot" adjustments for calibration are accessible by removing

the top or side panels. These controls should allow a rather large range of adjustment to accommodate changes in characteristics or constants at some later date.

All sections of the circuit that were not rather straightforward were breadboarded and demonstrated to work satisfactorily prior to drawing of the final schematic.

# APPENDIX C
# ALIASING TESTS

# APPENDIX C
# ALIASING TESTS

## INTRODUCTION

In order to supplement the analysis done on the SPND data channels, a test was conducted with a circuit that simulates the mathematical model of the analysis. The scope of this test was to input signals of known spectrum, and then qualitatively assess the degree of aliasing for different fs/fc ratios. The various spectrums were examined with an HP 3582 spectrum analyzer. Excessive aliasing is observed when the fundamental spectrum starts getting distorted from overlap with the first harmonic spectrum folding back. Figure C-1 illustrates a block diagram of a basic sample data system.

To model the situation with the TMI Data System, the Basic System of Figure C-1 was configured as shown in the block diagram of Figure C-2.

In order to simplify the instrumentation problem, the low-pass filter cut-off frequency was set at 100 Hz. This does not impact results since sample frequency was also set higher. Thus, the extent of aliasing can be accessed for various sample-frequency to cut-off-frequency ratios, including fs/fc = 2, which is the TMI case.

## TEST SETUP

The schematic for the test circuit is illustrated in Figure C-3. The low pass filter is realized as a simple, RC passive filter, with $f_c$ = 100 Hz. The impulse sampler is realized with the Datel Sample Hold Amplifier and the Harris Analog Switch. An external oscillator sets the sample frequency by triggering two 555 timers that in turn operate the sample hold amplifier and the analog switch. This circuitry models an ideal impulse sampler. The offset amplifier serves to introduce a dc signal to null out offsets introduced elsewhere; otherwise, the spectrum would have a large dc component. The input signal was provided by a sine wave generator

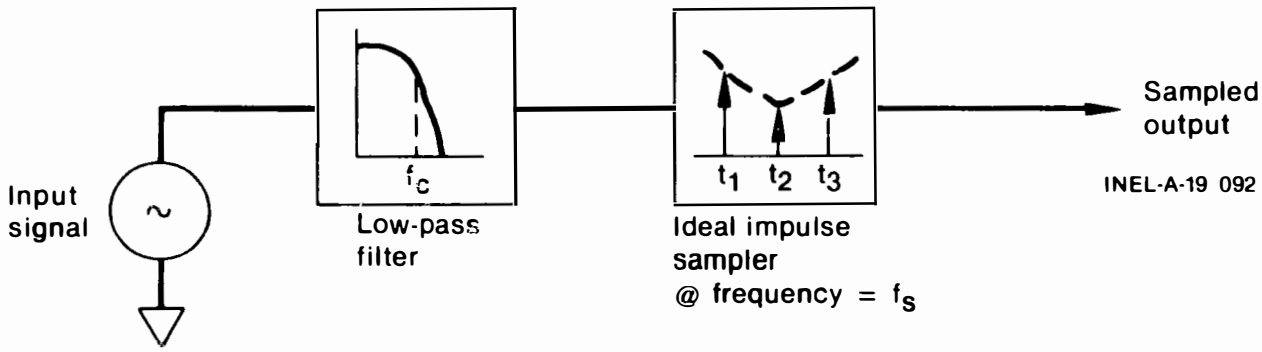


Figure C-1. The basic sample system.

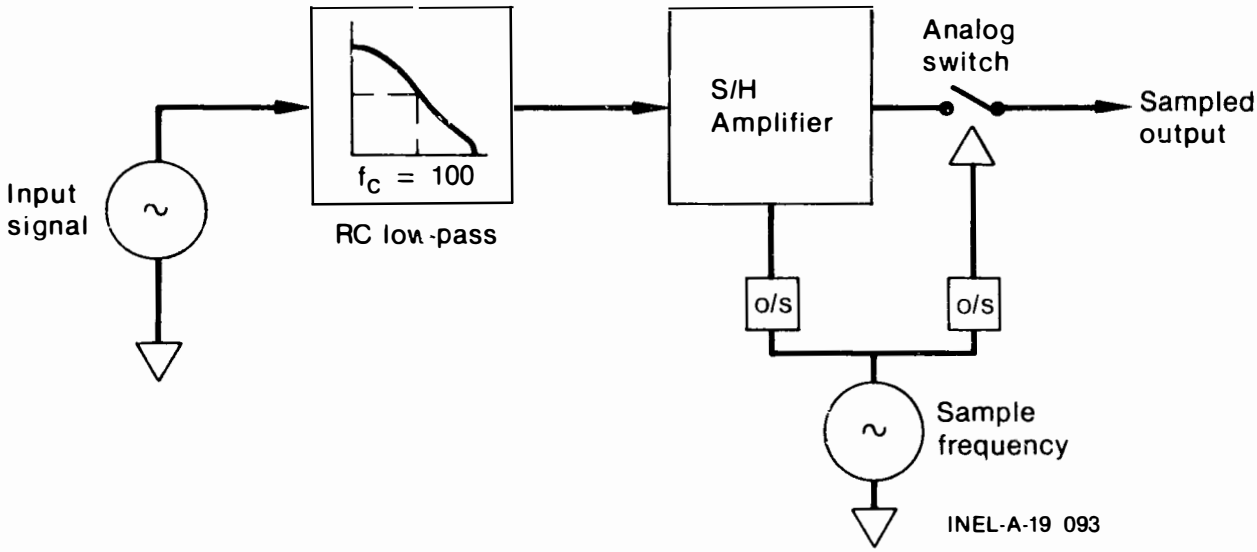


Figure C-2. Block diagram of impulse sampler.

1 msec/div

1 V/Div

Input = 100 Hz

Sample Rate = 500 Hz

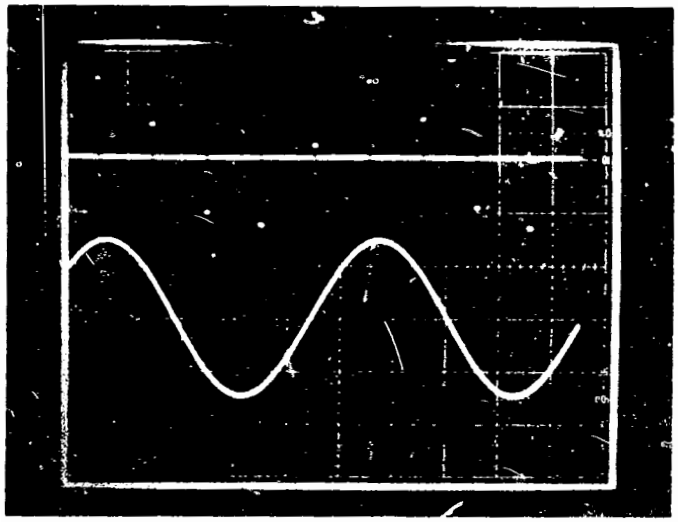

Figure C-3. Test circuit schematic.

and a random noise generator. Figure C-4 is a picture of an oscilloscope display with the top trace being the input sine curve and the bottom trace showing the resultant sampled wave form.

The final output from the analog switch was input into a spectrum analyzer. The analyzer calculates and displays the Fourier transform of the sampled wave form. The results one would expect with the spectrum of the sampled wave forms are illustrated in the following sketches. Figure C-5 illustrates the spectrum of some signal waveform with a cutoff frequency fc.

Figure C-6 is a sketch of the sampled spectrum at a frequency of fc = 5 fc. As seen in the sampled spectrum, the initial signal spectrum occurs and then repeats over and over again at harmonics of the sample frequency. Aliasing will occur when the sample frequency is not high enough, and the harmonic spectrums slide down and overlap the initial signal spectrum. Figure C-7 illustrates this case with fs = 3 fc. With no overlap, all the original information would be preserved. However, with overlap, the original spectrum is contaminated with the harmonic spectrum and information is lost. When the spectrums overlap they add together in the region of the overlap. Thus, for the case of Figure C-7, the resultant spectrum looks like the spectrum of white noise.

## TEST RESULTS

The first test that was run had a 100-Hz sine wave as the input signal. The sample frequency started at 500 Hz. The Figure C-8 shows the output of the spectrum analyzer as it analyzed the sampled sine wave shown in the first photo.

Some explanation is necessary with this photo. First, the camera chopped off the extreme right and the extreme left of the display. What is missing is a component of dc at the extreme left, which was the dc offset in the circuit. Thus, the signal component at 100 Hz is the first line on the left of the photo.

The fundamental spectrum looks like the sketch of Figure C-9.

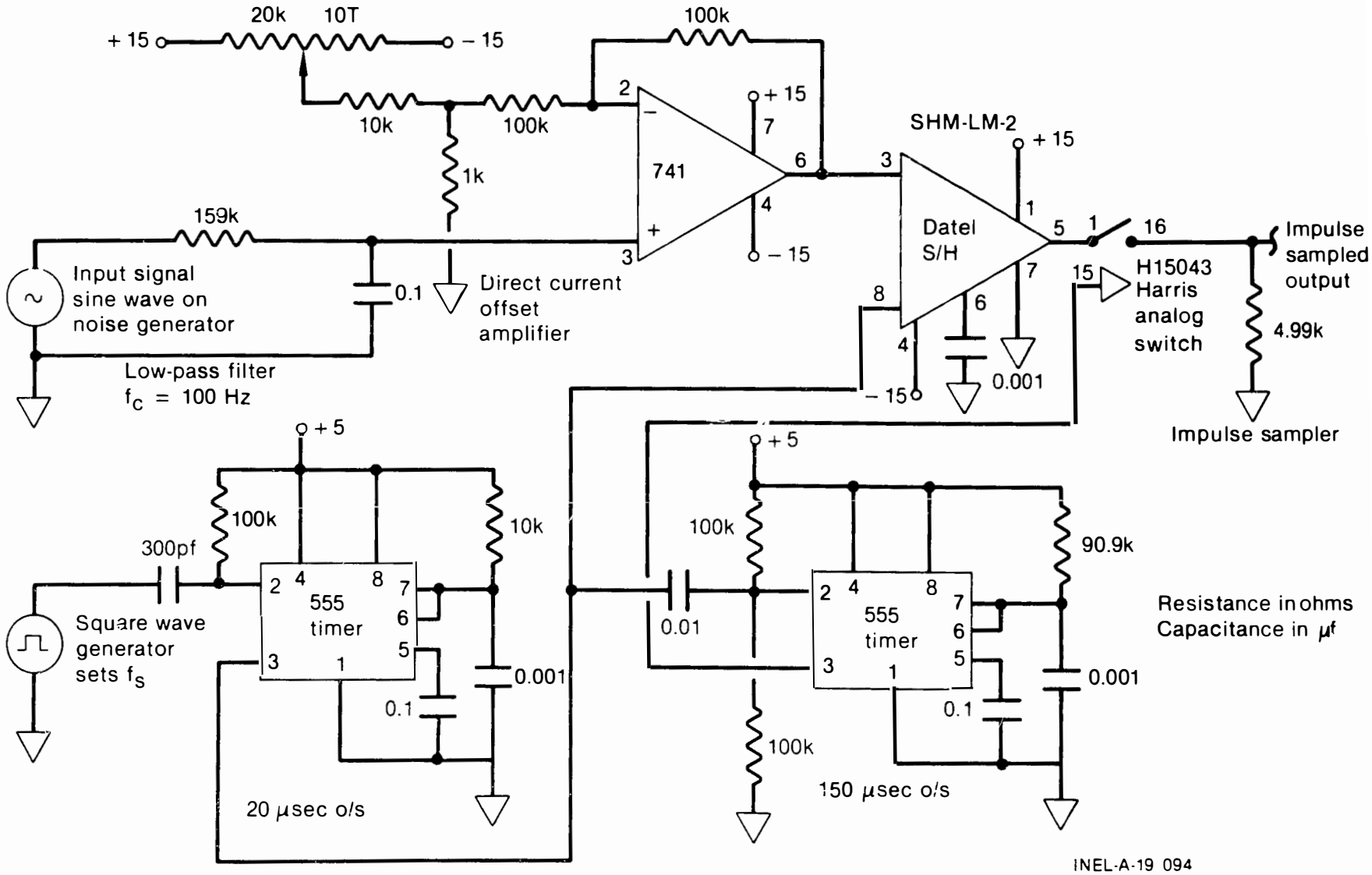


Figure C-4. Oscilloscope display of input sine wave and sampled sine wave.

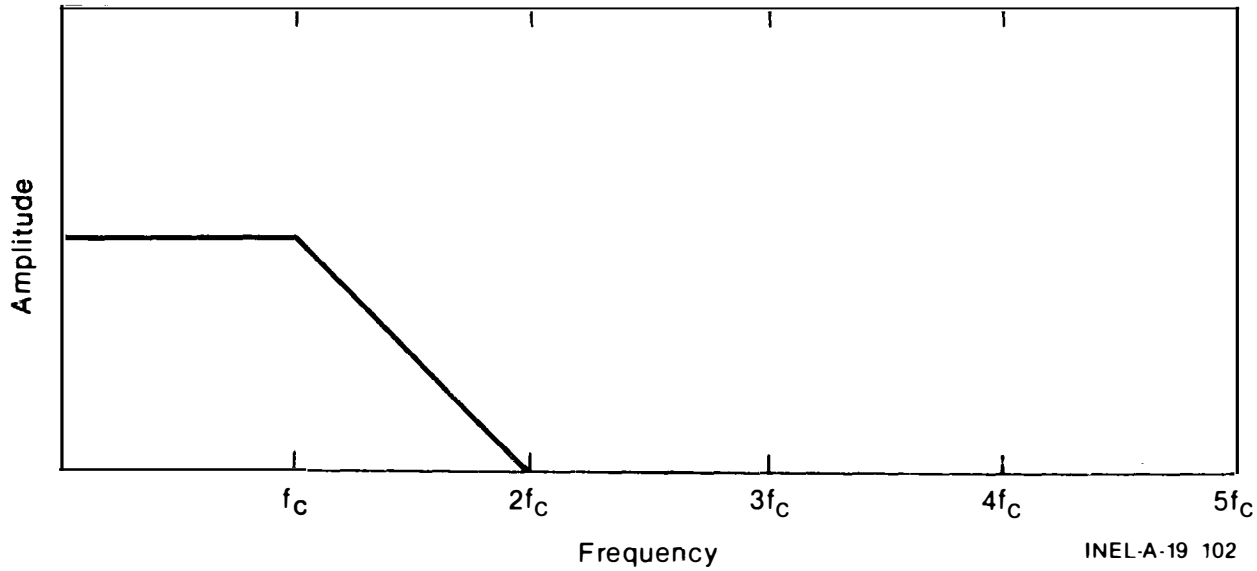


Figure C-5. Arbitrary signal spectrum.

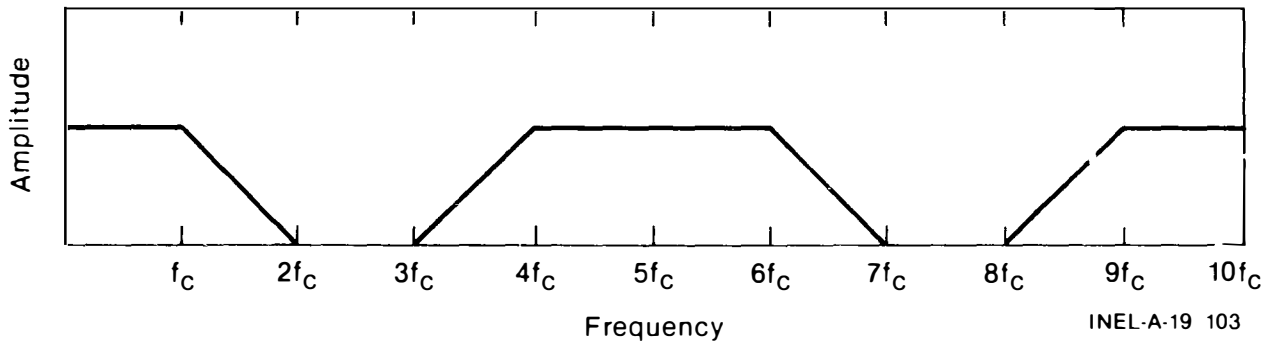


Figure C-6. Sampled signal spectrum sampled at fs = 5 fc.

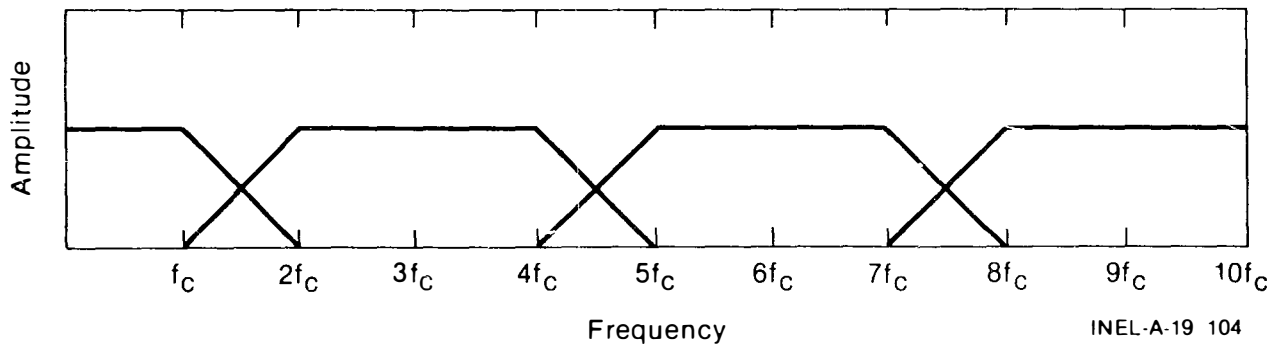


Figure C-7. Sampled signal spectrum sampled at fs = 3 fc.

Sinewave Frequency = 100 Hz

Sample Frequency = 500 Hz

Spectrum Frequency Range = 2.5 KHz

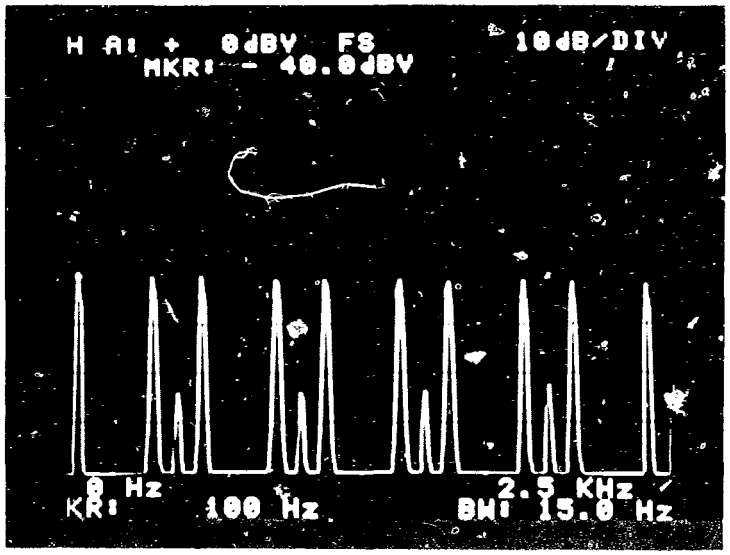


Figure C-8. Spectrum of sampled sine wave, 2.5 kHz range.

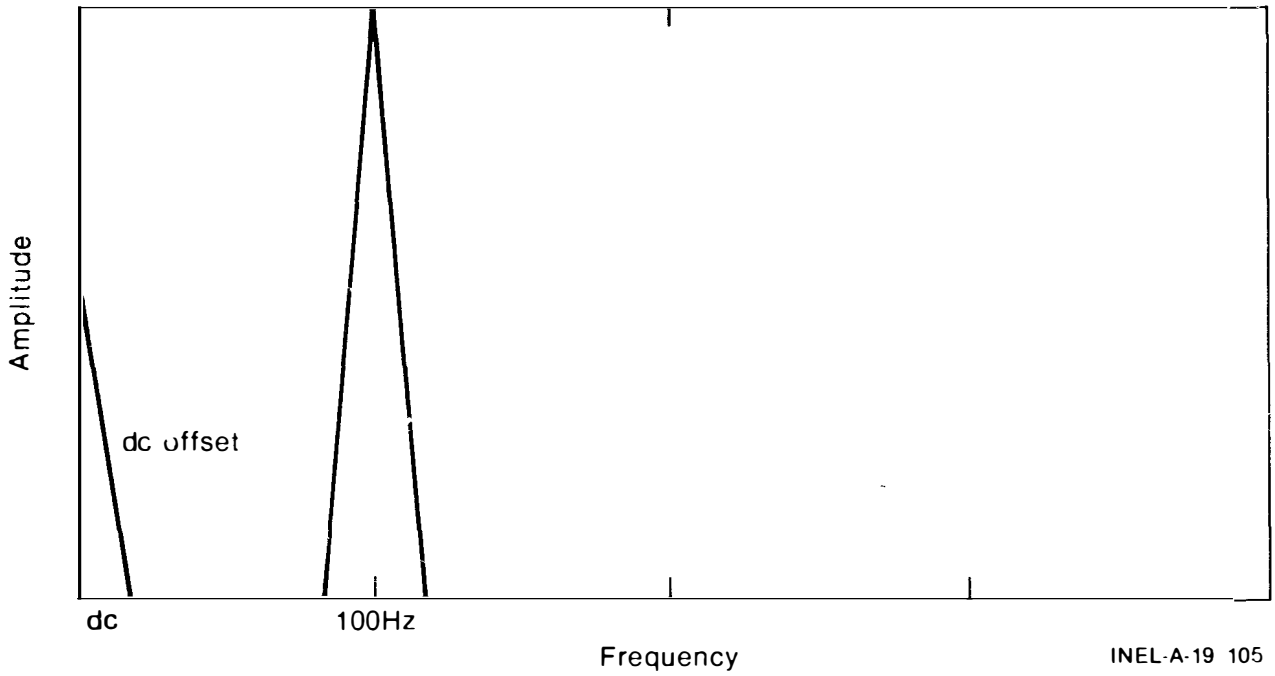


Figure C-9. Signal spectrum.

The harmonic spectrum that repeats at multiples of 500 Hz is shown in a sketch in Figure C-10.

With this explanation in mind, and referring to photograph C-8, the first harmonic spectrum occurs at 500 Hz. The second occurs at 1000 Hz, the third at 1500 Hz, the fourth at 2000 Hz, and finally only part of the fifth at 2500 Hz, which is the range of the spectrum. None of the harmonic or fundamental spectrums overlap. Figure C-11 shows the same thing as Figure C-8, except with a blown-up frequency scale of 500 Hz. Thus, only the lower half of the first harmonic shows up.

In Figure C-12, the sample frequency was reduced to 350 Hz and, as one would predict, the first harmonic spectrum has moved down scale, now occuring at 350 Hz. The frequency range is still at 500 Hz.

In Figure C-13, the sample frequency was reduced to 250 Hz. The first harmonic spectrum has moved further down scale and is close to overlap.

In Figure C-14, the sample frequency was reduced to 200 Hz, which is just twice the signal frequency. At this point, the lower part of the harmonic spectrum has coincided with the fundamental spectrum.

In Figure C-15, the sample frequency was reduced to 150 Hz. The lower part of the harmonic spectrum has moved down to 50 Hz. Thus, as the sample rate falls off, the harmonic spectrum moves down into the signal spectrum and contaminates it with aliasing.

Two more photographs with sine wave excitation are of interest. They show in the time domain with the 100 Hz sine wave being sampled at a 200 Hz rate. In Figure C-16, the samples have occurred near peak voltage. However, in Figure C-17, the samples have occurred near crossover, and they show no output. These two photographs should illustrate why, if the system samples are at twice the highest frequency, that frequency cannot be resolved with any certainty.

The second test run utilized a random noise source as signal excitation. Recall from system theory that the average spectrum of a white noise

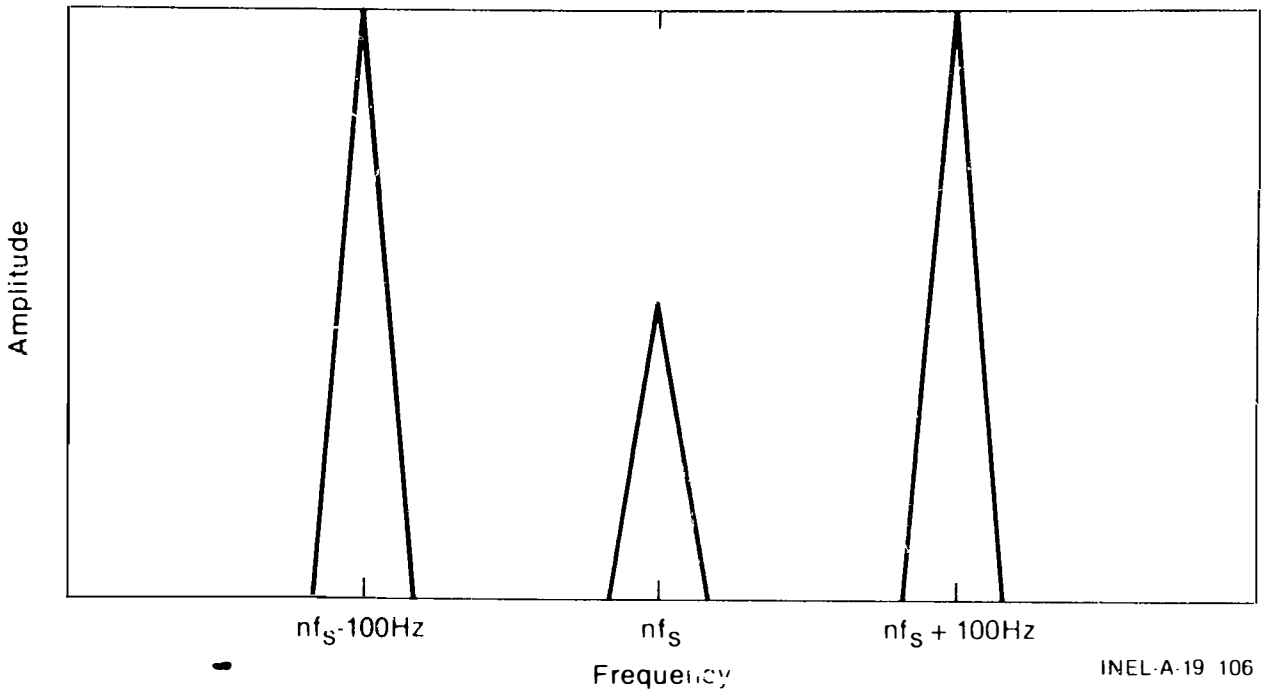


Figure C-10. The harmonic spectrum.

Sine Wave Frequency = 100 Hz
Sample Frequency = 500 Hz
Frequency Range = 500 hz

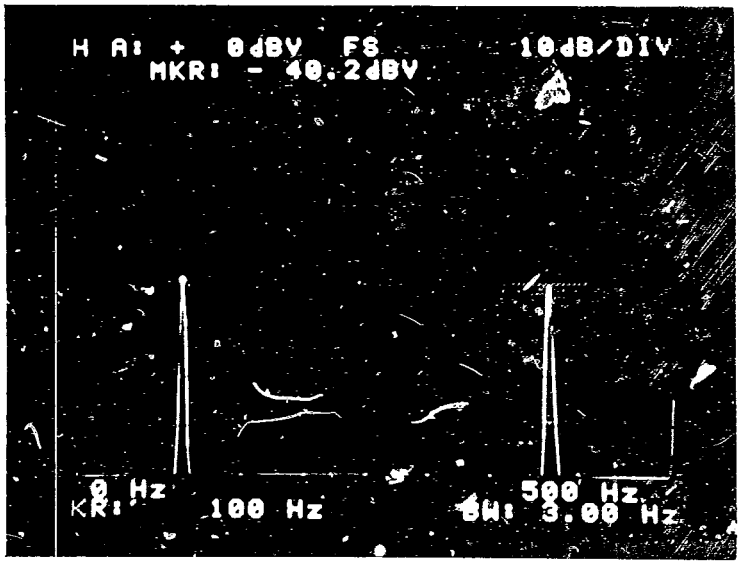


Figure C-11. Spectrum of sampled sine wave, 500 Hz range.

Sine Wave Frequency = 100 Hz
Sample Frequency = 350 Hz
Frequency Range = 500 Hz

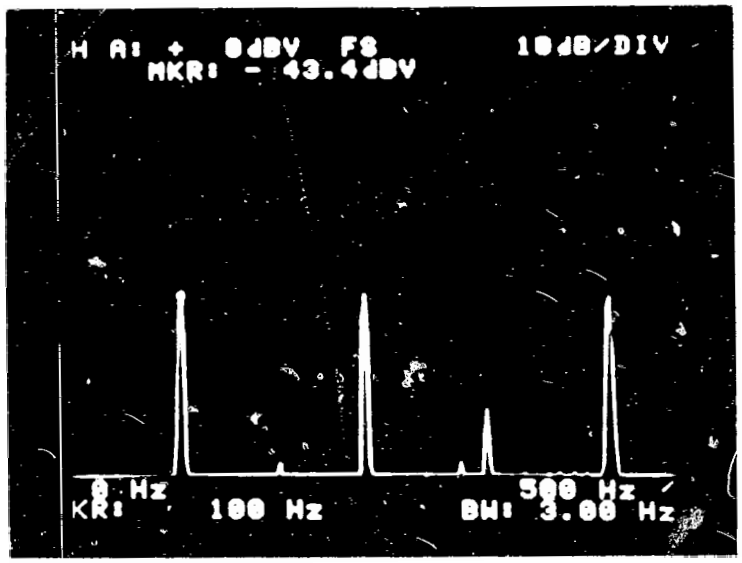


Figure C-12. Spectrum of sampled sine wave, sample frequency 350 Hz range.

Sine Wave Frequency = 100 Hz
Sample Frequency = 250 Hz
Frequency Range = 500 Hz

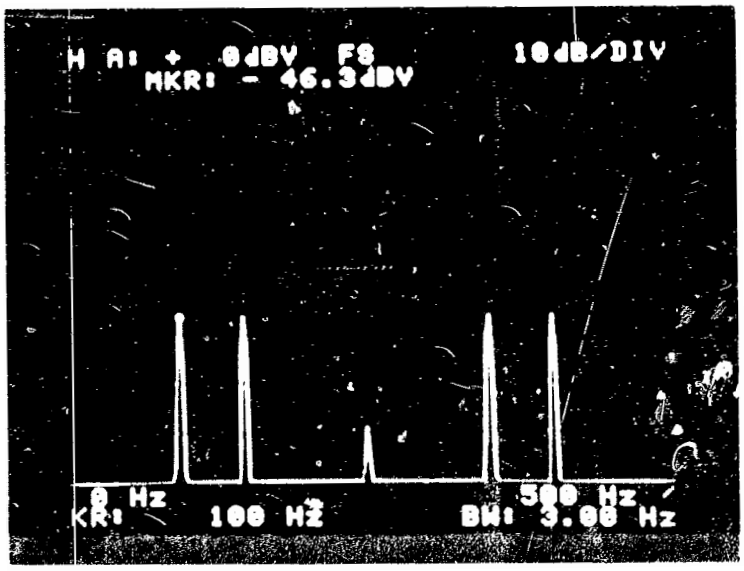


Figure C-13. Spectrum of sampled sine wave, sample frequency 250 Hz range.

Sine Wave Frequency = 100 Hz

Sample Frequency = 200 Hz

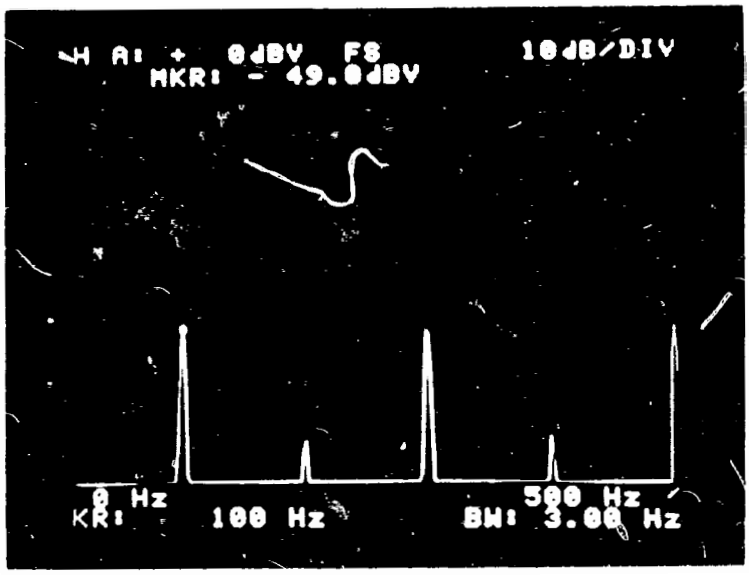


Figure C-14. Spectrum of sampled sine wave, sample frequency 200 Hz range.

Sine Wave Frequency = 100 Hz

Sample Frequency = 150 Hz

Frequency Range = 500 Hz


Figure C-15. Spectrum of sampled sine wave, sample frequency 150 Hz range.

1V/Div, 2 msec/div

Sine Wave Frequency = 100 Hz

Sample Rate - 200 Hz

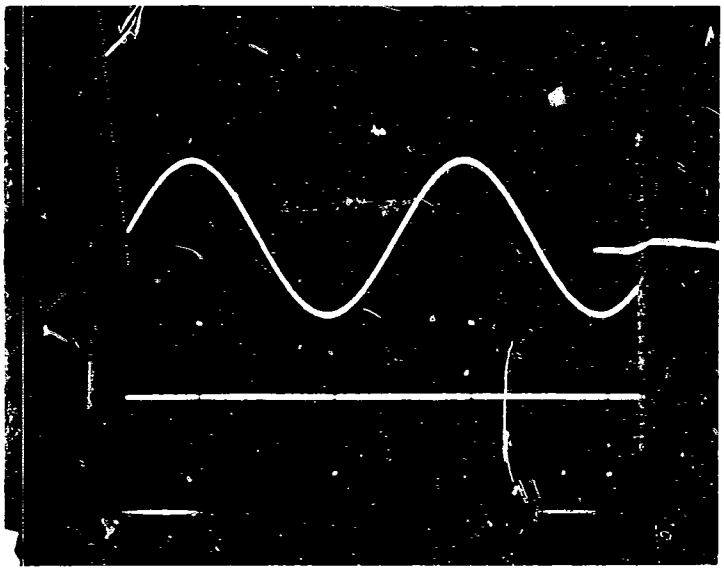

Figure C-16. Oscilloscope trace of sampled sine wave, 200 Hz near peak voltage.

1V/div, 2 msec/div

Sine Wave Frequency = 100 Hz

Sample Rate = 200 Hz

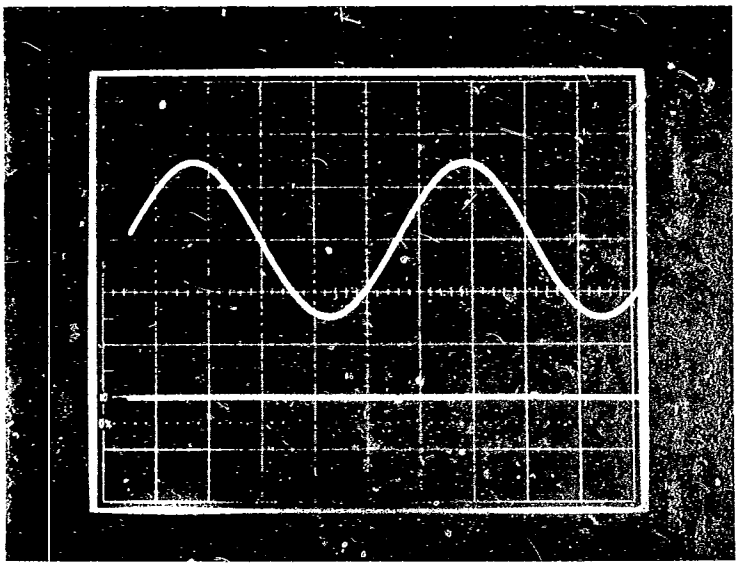

Figure C-17. Oscilloscope trace of sampled sine wave, 200 Hz range near crossover.

source is the same as the spectrum of an impulse. The response of a system in the frequency domain is the spectrum of the system's impulse response. However, ideal impulses are difficult to realize. If, on the other hand, a system were excited with white noise, and the spectrum of the systems response to the noise were averaged, the result would be the same as the impulse response. Therefore, exciting the system with random noise should provide a clear and appropriate demonstration of the aliasing problem.

The first photograph with the noise excitation, Figure C-18, shows the spectrum of the response of the low-pass filter. The filter shown in the test circuit schematic had a cutoff frequency of 100 Hz. Observe how the low-pass first order does not roll off quickly. One would expect overlap from the harmonics in the sampled spectrum to become significant at sample rates above 200 Hz.

In Figure C-19, a spectrum of the filter response is overlaid with a sampled response with fs = 500 Hz. As seen in the photograph, the sampled spectrum is distorted by the first harmonic at around 200 Hz. The spikes are caused by dc offsets.

Figure C-20 is the same as C-19, except the sample rate was reduced to 350 Hz. Distortion after 144 Hz is significant.

Figure C-21 shows the sampled spectrum alone for a sample rate of 200 Hz. As can be observed, it no longer resembles any part of the low pass spectrum. Figure C-22 shows the oscilloscope trace of the noise signal and samples.

## CONCLUSIONS

As can be seen from the various tests, in order to establish an acceptable level of aliasing in a sample data system the parameters of bandwidth, sample rate, and roll off rate must be carefully chosen.

Frequency Range = 1 KHz

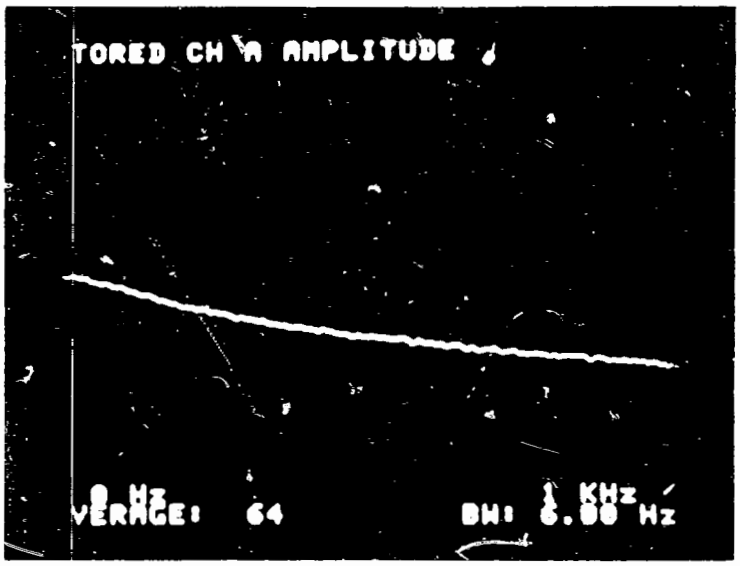


Figure C-18. Low-pass filter spectrum with random noise input.

Sample Rate = 500 Hz

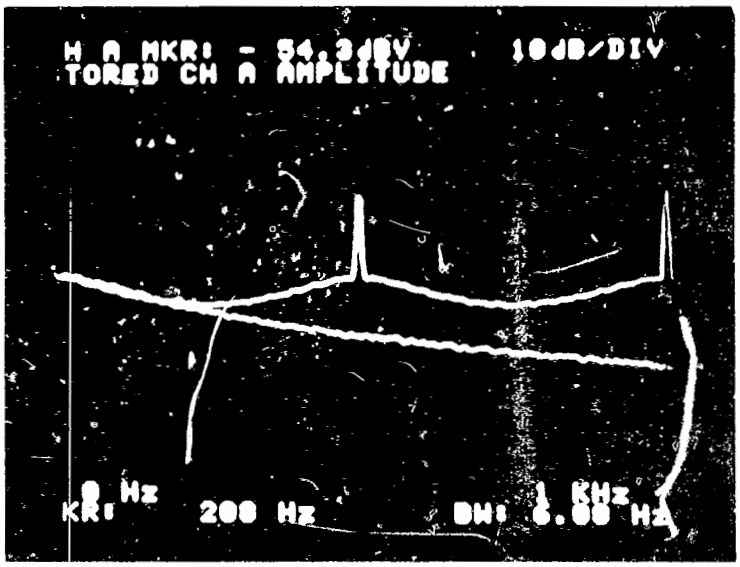


Figure C-19. Low-pass filter sampled spectrum overlay on unsampled spectrum.

Sample Rate = 350 Hz

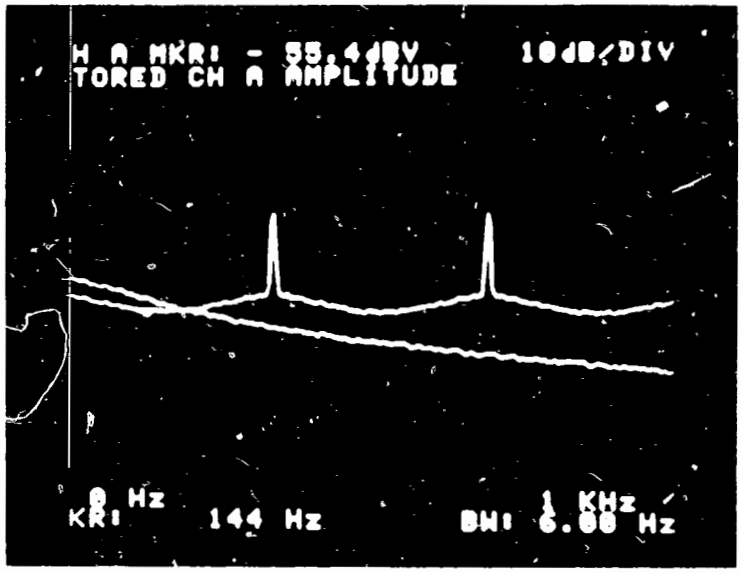


Figure C-20. Low-pass filter sample spectrum overlay.

Sample Rate = 200 Hz

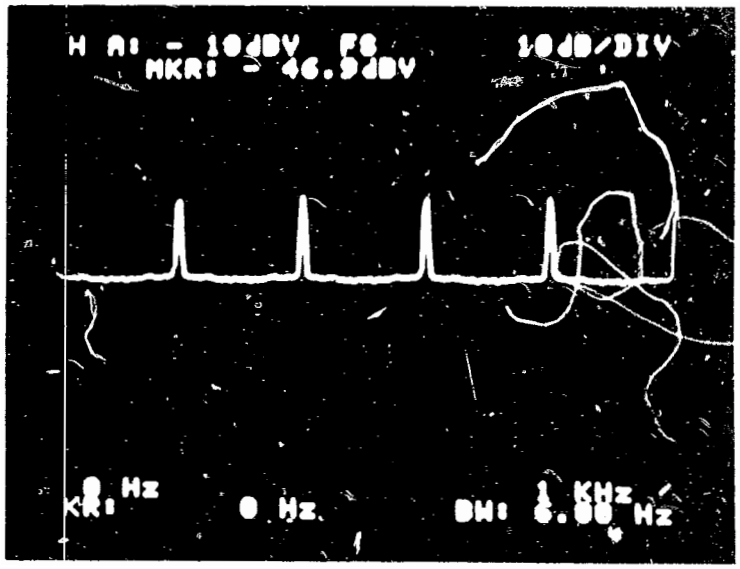


Figure C-21. Low-pass filter sampled spectrum with random noise input.

1V/div, 2 msec/div
Sample Rate = 500 Hz

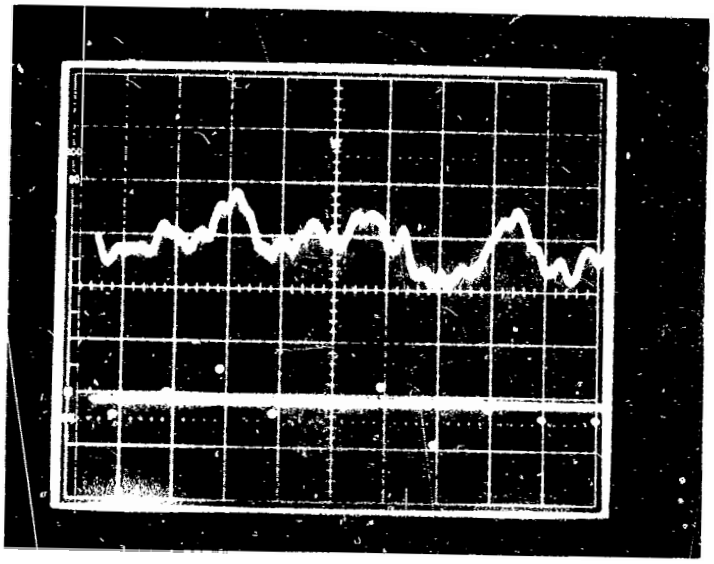

Figure C-22. Oscilloscope photo of noise and sampled noise.